Coordination of Smart Hybrid Transformers in Distribution Networks

Samuel Hayward, Michael Merlin, *Member, IEEE,* Matthew Williams, and Thomas Morstyn, *Senior Member, IEEE*

***Abstract*—A hybrid transformer is a combination of a conventional transformer and power electronics, which can be used to help alleviate power quality issues in distribution networks at lower costs than solid-state transformers. This paper proposes a novel method of coordinating multiple hybrid transformers in 3-phase distribution networks in order to reduce the curtailment of distributed generators. This is accomplished through the use of sequential linear programming, key features of which include accounting for the nonlinear voltage control capabilities of hybrid transformers, and managing the nonlinear constraints of hybrid transformer power electronics. Test cases were carried out in a modified unbalanced version of the IEEE 69-Bus network and a reduced version of the European Low Voltage test feeder. Test case results demonstrate that hybrid transformers can substantially increase the utilisation of distributed generators.**

***Index Terms*—hybrid transformer, optimal power flow, power injection model, power quality, renewable distributed generation, sequential linear programming, successive linear programming, voltage control, voltage source model.**

NOMENCLATURE.

List of Sets

$\mathcal{N}$	Set of network buses (excluding the grid-connected slack bus).
$\mathcal{N}^{DG}$	Set of network buses that have DG units.
$\mathcal{N}^{HTp}$	Set of HT virtual buses.
$\mathcal{N}^{HTs}$	Set of HT LV buses.
$\mathcal{N}^{Y}$	Set of wye-connected network buses (subset of $\mathcal{N}$).
$\mathcal{N}^{\Delta}$	Set of delta-connected network buses (subset of $\mathcal{N}$).
ε^{HT}	Set of lines between HT virtual buses and LV buses (where (i, j) denotes a line from virtual bus i to LV bus j).
Ω	Set of network phases (i.e., 0, 1, 2).

List of Nodal Admittance Matrix Variables

$\overline{Y}_I \in \mathbb{C}^{3x3}$	Submatrix of $\overline{Y}_{Node}$.
$\overline{Y}_{Node} \in \mathbb{C}^{6x6}$	Three-phase transformer nodal admittance matrix.
$y_t \in \mathbb{C}$	Per phase transformer leakage admittance.

List of Optimisation Constants

$B_{ij} \in \mathbb{R}^{\Omega\times\Omega}$	Susceptance matrix for the line between virtual bus i and LV bus j of a Hybrid Transformer.
$C_1 \in \mathbb{R}$	Constant used to reduce results of Optimal Power Flow constraint (22.41) to ensure feasible results.
$G_{ij} \in \mathbb{R}^{\Omega\times\Omega}$	Conductance matrix for the line between virtual bus i and LV bus j of a Hybrid Transformer.
$K^0 \in \mathbb{R}^{3\mathbb{N}}$	Linear network model zero-load voltage magnitude vector.
$K^Y \in \mathbb{R}^{3\mathbb{N}\times6\mathbb{N}}$	Linear network model coefficient matrix for power injections made at wye-connected buses to calculate voltage magnitudes.
$K^{\Delta} \in \mathbb{R}^{3\mathbb{N}\times6\mathbb{N}}$	Linear network model coefficient matrix for power injections made at wye-connected buses to calculate voltage magnitudes.
$M^0 \in \mathbb{R}^{3\mathbb{N}}$	Linear network model zero-load complex voltage vector.
$M^Y \in \mathbb{R}^{3\mathbb{N}\times6\mathbb{N}}$	Linear network model coefficient matrix for power injections made at wye-connected buses to calculate complex voltages.
$M^{\Delta} \in \mathbb{R}^{3\mathbb{N}\times6\mathbb{N}}$	Linear network model coefficient matrix for power injections made at delta-connected buses to calculate complex voltages.
$\overline{P_i} \in \mathbb{R}$	Maximum allowable active power output for DG connected at network bus i.
$PF_i \in \mathbb{R}$	Power factor for DG connected at network bus i.
$\overline{S}_{ij} \in \mathbb{R}$	Maximum apparent power rating for Hybrid Transformer power electronic converters.
$s^{base} \in \mathbb{R}$	Base apparent power for network.
$stp_i^{DG} \in \mathbb{R}$	Step-size restriction for DG active power output at network bus i.
$stp^{v} \in \mathbb{R}$	Step-size restriction for Hybrid Transformer voltage compensation.
$stp^{\gamma} \in \mathbb{R}$	Step-size restriction for Hybrid Transformer phase shifting.

Samuel Hayward is with the University of Edinburgh, Edinburgh, United Kingdom (email: s1547241@ed.ac.uk).

Michael Merlin is with the University of Edinburgh, Edinburgh, United Kingdom (email: michael.merlin@ed.ac.uk).

Mattew Williams is with the private company IONATE, Edinburgh, United Kingdom (email: matthew@ionate.energy).

Thomas Morstyn is with the University of Oxford, Oxford, United Kingdom (email: thomas.morstyn@eng.ox.ac.uk).

This work was supported by the Scottish Government and IONATE through the ETP Energy Industry Doctorate Programme (project reference 180) and by the Engineering and Physical Sciences Research Council (EPSRC) (project reference EP/X027384/1).

$\lvert\underline{v}\rvert, \lvert\overline{v}\rvert \in \mathbb{R}$	Minimum and maximum allowable network phase voltages.
$v^{base} \in \mathbb{R}$	Base voltage for network.
$w_1, w_2 \in \mathbb{R}$	Weights applied in Optimal Power Flow's objective function to discourage unnecessary utilisation of Hybrid Transformers.
$x^Y \in \mathbb{R}^{6\mathcal{N}}$	Uncontrollable network power injections at wye-connected buses.
$x^\Delta \in \mathbb{R}^{6\mathcal{N}}$	Uncontrollable network power injections at delta-connected buses.

Other optimisation constants include the nominal operating points for optimisation decision variables. The notation $a^{(k)}$ is used to denote nominal operating point constants for the optimisation in iteration k of the sequential linear program (e.g., $e_{ij,\phi}^{pq,(k)}$ is the nominal operating point for the decision variable $e_{ij\phi}^{pq}$).

List of Optimisation Variables

$e \in \mathbb{R}^{3\mathcal{N}}$	Real network phase voltages.
$e_{ij}^{abs} \in \mathbb{R}^{\Omega}$	Magnitude of e_{ij}^{pq}.
$e_{ij}^{pq} \in \mathbb{R}^{\Omega}$	Real compensating voltage of the Hybrid Transformer with virtual bus i and LV bus j.
$f \in \mathbb{R}^{3\mathcal{N}}$	Imaginary network phase voltages.
$f_{ij}^{abs} \in \mathbb{R}^{\Omega}$	Magnitude of f_{ij}^{pq}.
$f_{ij}^{pq} \in \mathbb{R}^{\Omega}$	Imaginary compensating voltage of the Hybrid Transformer with virtual bus i and LV bus j.
$P_i^{DG} \in \mathbb{R}^{\Omega}$	Active power output of DG connected at network bus i.
$P_{ij}^{pri} \in \mathbb{R}^{\Omega}$	Active power injections made at Hybrid Transformer virtual bus i.
$P_{ij}^{se} \in \mathbb{R}^{\Omega}$	Active power injections made at Hybrid Transformer LV bus j due to voltage compensation.
$P_{ij}^{sec} \in \mathbb{R}^{\Omega}$	Overall active power injections made at Hybrid Transformer LV bus j.
$P_{ij}^{sh} \in \mathbb{R}^{\Omega}$	Active power exchange between the series and shunt converters of a Hybrid Transformer with virtual bus i and LV bus j.
$\lvert\overline{Q}_{ij}\rvert \in \mathbb{R}^{\Omega}$	The magnitudes of the maximum reactive power that can be present in the power electronic converters of the Hybrid Transformer with virtual bus i and LV bus j.
$Q_{ij}^{abs} \in \mathbb{R}^{\Omega}$	Magnitude of Q_{ij}^{sh}.
$Q_{ij}^{c} \in \mathbb{R}^{\Omega}$	Reactive power in the series converter of the Hybrid Transformer with virtual bus i and LV bus j.
$Q_i^{DG} \in \mathbb{R}^{\Omega}$	Reactive power output of DG connected at network bus i.
$Q_{ij}^{pri} \in \mathbb{R}^{\Omega}$	Reactive power injections made at Hybrid Transformer virtual bus i.
$Q_{ij}^{se} \in \mathbb{R}^{\Omega}$	Reactive power injections made at Hybrid Transformer LV bus j due to voltage compensation.
$Q_{ij}^{sec} \in \mathbb{R}^{\Omega}$	Overall reactive power injections made at Hybrid Transformer LV bus j.
$Q_{ij}^{sh} \in \mathbb{R}^{\Omega}$	Reactive power provided by the shunt converter of the Hybrid Transformer with virtual bus i and LV bus j.
$r_{ij} \in \mathbb{R}^{\Omega}$	Magnitude of the Hybrid Transformer compensating voltage relative to v_i.
$v \in \mathbb{C}^{3\mathcal{N}}$	Complex network phase voltages.
$\lvert v\rvert \in \mathbb{R}^{3\mathcal{N}}$	Network phase voltage magnitudes.
$\gamma_{ij} \in \mathbb{R}^{\Omega}$	Phase shift angle for the Hybrid Transformer compensating voltage.
$\Delta p^Y \in \mathbb{R}^{3\mathcal{N}}$	Controllable network active power injections at wye-connected buses.
$\Delta p^\Delta \in \mathbb{R}^{3\mathcal{N}}$	Controllable network active power injections at delta-connected buses.
$\Delta q^Y \in \mathbb{R}^{3\mathcal{N}}$	Controllable network reactive power injections at wye-connected buses.
$\Delta q^\Delta \in \mathbb{R}^{3\mathcal{N}}$	Controllable network reactive power injections at delta-connected buses.
$\Delta x^Y \in \mathbb{R}^{6\mathcal{N}}$	Controllable network power injections at wye-connected buses.
$\Delta x^\Delta \in \mathbb{R}^{6\mathcal{N}}$	Controllable network power injections at delta-connected buses.

List of Accuracy Check Variables

$S_{ij}^{c} \in \mathbb{R}^{\Omega}$	Apparent power through the Hybrid Transformer series converter.
$S_{ij}^{pri} \in \mathbb{C}^{\Omega}$	Apparent power injection made at Hybrid Transformer virtual bus i.
$S_{ij}^{se} \in \mathbb{C}^{\Omega}$	Apparent power injection made at Hybrid Transformer LV bus j due to voltage compensation.
$v_{ij}^{pq\ act} \in \mathbb{C}^{\Omega}$	Averaged value of v_{ij}^{pq1} and v_{ij}^{pq2}.
$v_{ij}^{pq\ OPF} \in \mathbb{C}^{\Omega}$	Hybrid Transformer compensating voltage predicted by the Optimal Power Flow method.
v_{ij}^{pq1}, $v_{ij}^{pq2} \in \mathbb{C}^{\Omega}$	Hybrid Transformer compensating voltages calculated from the power flow results.
$v_{ij}^{sum} \in \mathbb{R}$	Sum of all Δv_{ij}^{pq} for all phase in Ω.
$v^{tol} \in \mathbb{R}$	Hybrid Transformer voltage compensation error tolerance.
$Z_{ij}^{HT} \in \mathbb{C}^{\Omega\times\Omega}$	Impedance matrix for the line between virtual bus i and LV bus j of a Hybrid Transformer.
$\Delta v_{ij}^{pq} \in \mathbb{R}^{\Omega}$	Difference in magnitude between $v_{ij}^{pq\ act}$ and $v_{ij}^{pq\ OPF}$.

I. INTRODUCTION.

In recent years, governments across the world have set goals to reduce the emission of greenhouse gases as a means of combatting climate change. This has resulted in increasing penetration of renewable distributed generators (DG) in electrical distribution networks [1], [2], [3], [4]. An example of this is that global distributed solar photovoltaic (PV) capacity increased by 366.4GW between the years 2017 and 2022, and is set to increase by an additional 1139.9GW by 2028 [5]. However, renewable DGs can cause power quality issues, such as voltage fluctuations and poor

power factors, which can impact the reliability of distribution networks [1], [2], [4]. One potential solution to alleviate these power quality issues is to reinforce the distribution networks. However, this method is expensive and time intensive [1]. Another solution is to integrate volt/VAR control devices into distribution networks [6]. Devices capable of mitigating these power quality issues include transformers with On-Load Tap Changers (OLTC), Solid-State Transformers (SST), and Hybrid Transformers (HT) [6], [7].

An OLTC adjusts the turn ratio of a transformer by connecting to different parts of the transformer coils in order to control the output voltage [8]. OLTCs provide transformers with additional controllability without significantly reducing efficiency or reliability of the transformer [9]. However, OLTCs quickly wear down if forced to change tap position too frequently within a short period of time [10], [11]. Typically, an OLTC will only adjust its tap position a few times per day, which is not frequent enough to handle the continuous changes to voltage levels caused by DGs [3], [12]. Furthermore, OLTCs can only adjust voltage in discrete steps (e.g., 2% voltage change per tap), whereas SSTs and HTs have more precise dynamic voltage regulation capability, which allows for greater flexibility [6]. Therefore, OLTCs are not an ideal solution for the power quality issues caused by renewable DG in distribution grids.

SSTs are power electronic devices that are able to provide full control over the terminal voltages and currents and, therefore, full control over the active and reactive power flows [9], [3]. However, SSTs are very expensive due to the high power rating of their power electronics and they tend to have a shorter operational lifespan than conventional power transformers [1], [9], [3], [13]. Additionally, transformers in distribution networks are required to withstand large spikes in voltage and current for certain periods of time (e.g., the maximum rated short circuit current for 2 seconds) [14]. However, an SST's power electronics are vulnerable to large spikes in voltage and current, and can only withstand such spikes for much shorter periods of time (e.g., 10 to 50 milliseconds) [3], [14]. It is possible for SSTs to be designed to be able to better withstand overvoltages and overcurrents, and if an SST is still vulnerable, then external protection devices such as surge arrestors, fuses, diodes, and bidirectional solid-state circuit breakers can also be implemented into the SST [15], [16]. However, such design decisions and protection devices can increase SST costs [16]. These limitations have prevented the widespread adoption of SSTs within distribution networks.

An HT is the combination of a conventional transformer and fractionally rated power electronics [1], [2]. An HT's power electronics provide control capabilities such as dynamic voltage regulation and power factor correction [1]. Since HT power electronics are only rated for a fraction of the transformer's total transferable power (typically 10-20%) they provide less controllability than SSTs, which have power electronics that are rated for the total transferable power [1], [17]. However, the controllability provided by HTs is still sufficient for mitigating power quality issues. Furthermore, unlike SSTs, HTs can still operate even if their power electronics fail by bypassing its power electronics and operating as a conventional transformer [1], [2]. A typical power transformer has an overall efficiency of 99% [9], [3]. However, due to the addition of power electronic converters, HTs are less efficient than conventional power transformers, potentially ranging from an overall efficiency of 98.6% to 98.9% [3]. HTs are still more efficient than SSTs, which can have an overall efficiency of approximately 97% [9], [3], [13]. In terms of material costs, both HTs and SSTs are more expensive than conventional power transformers due the inclusion of power electronics [3]. HTs, due to the fact that their power electronics are fractionally rated instead of fully rated, are cheaper than SSTs, which can potentially cost up to 5 to 25 times more than conventional transformers [1], [9], [3], [14]. It is also possible that the additional control capabilities of HTs and SSTs may be able to help offset their greater material costs, however, the economic impact of HTs and SSTs have yet to be examined in great detail. One disadvantage HTs have in comparison to conventional power transformers and SSTs is volume. HTs tend to have a larger volume than similarly rated conventional transformers (due to the addition of the power electronics) and SSTs (which have a lower volume than conventional transformers) [3]. Overall, HTs are an appealing choice for implementation in distribution grids when compared to OLTCs and SSTs, offering a balance between controllability, robustness, efficiency, and cost.

There already exists methods and techniques for coordinating volt/VAR control devices with one another to control network voltages and allow for more DG implementation. For example, in [18] and [19] a branch-flow model optimal power flow (OPF) method which coordinates step-voltage regulator (SVR) tap positions is presented, [20] discusses an OPF that has OLTC tap positions as decision variables, and in [21] an OPF that coordinates reactive power compensators and OLTC tap positions is described. However, to the authors' best knowledge, there has been no work on the optimisation of multiple HTs in a distribution network. Prior work and research done with HTs has primarily focused on the modelling, simulation, and/or testing of single HTs within specific test cases. In [1] the setup and results of a benchtop HT prototype are presented, and the plans for field testing an HT are also presented along with preliminary field results. In [4] the design and simulation results for a novel Open-Winding HT (OWHT) are demonstrated. In [22] the concept, laboratory prototype, and simulation results of a single HT with a matrix converter are shown. As previously mentioned, HTs are a potential solution to power quality issues caused by DG integration, and, furthermore, the coordination of multiple HTs can provide greater control over a network and allow for even greater DG integration than with a single HT. However, from what has been shown in the reviewed literature there seems to be a lack of optimisation methods which can demonstrate the potential benefits of

the integration and control of HTs in distribution networks. Therefore, this motivates the need for the development of such optimisation methods, so that the potential benefits of HT integration and coordination can be more fully explored during the planning and simulation of distribution networks.

The novel contribution of this paper is a Sequential Linear Programming (SLP) technique that has been developed in order to coordinate multiple HTs within distribution networks, referred to as the HT SLP. An SLP technique was chosen because it addresses the nonlinear characteristics and constraints of HTs and distribution networks by iteratively solving a series of Linear Programming (LP) problems without the need to solve a Nonlinear Programming (NLP) problem, as described in further detail in Section III. Fast and reliable optimisation solvers are widely available for LPs, and therefore, using SLP helps to ensure that the utilisation of the optimisation method for coordinating HTs is not restricted by the choice of optimisation solver. The proposed HT SLP method is able to account for the nonlinear characteristics of HT models, and works with unbalanced, multi-phase distribution network models. The proposed HT SLP method was tested in a case study with a version of the IEEE 69-Bus network that has been modified to be unbalanced, and another case study with the IEEE European Low Voltage (EULV) test feeder. Test case results show that the proposed HT SLP method can successfully coordinate HTs in an unbalanced multi-phase networks to maximise DG output.

In this paper, Section II explains how HTs are modelled for steady-state power flow simulations. Section III describes the HT SLP method. Section IV details the modified IEEE 69-Bus network and EULV test feeder used as test cases for the proposed HT SLP method, and describes the results of the test cases, demonstrating that the proposed HT SLP method can successfully coordinate HT models in order to prevent DG curtailment within both test networks. Section V concludes the paper. Appendix A describes an alternative SLP method that maximises DG output without utilising the HT models present within the test case networks, referred to as the No-HT SLP, which is used to help demonstrate the impact of HT utilisation.

II. HYBRID TRANSFORMER MODEL.

The proposed HT SLP method in this paper focuses on utilising HT models to provide volt/VAR control, specifically to maximise DG output. This can be accomplished through static network modelling. Therefore, the HT models presented here in this section are quasi-static models.

As previously mentioned, an HT is a combination of a conventional transformer and power electronics. There are numerous different topologies for HTs, where the transformer and power electronics connect with one another in different ways [2], [17]. However, for this paper it is assumed that the HT is a three-winding transformer connected to a pair power electronic converters, where one converter connects to the transformer in series via the tertiary winding and the other

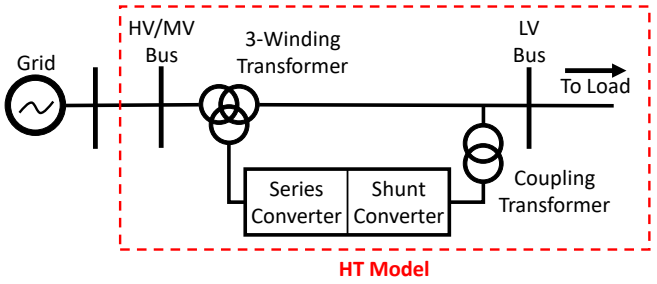

Fig. 1: Single line diagram of the three-winding transformer HT model.

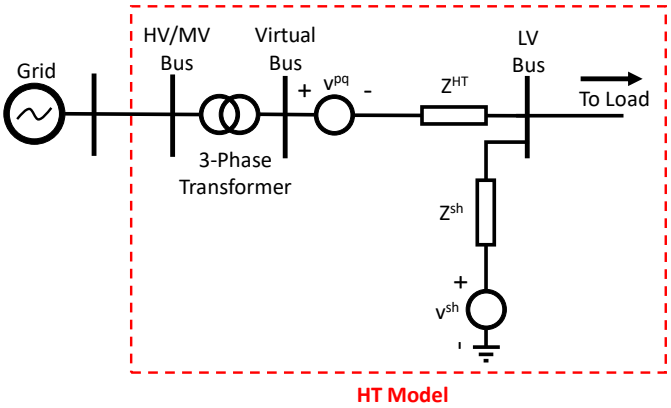

Fig. 2: Single line diagram of the HT VSM.

connects to the transformer's output via a shunt connection (as shown in Figure 1). For distribution HTs, the shunt connection can either be a direct coupling or done through a coupling transformer, depending on whether voltage levels need to be adjusted for the shunt converter. For this paper, it is assumed that the shunt connection is achieved through a coupling transformer. This HT is only capable of generating reactive power, no active power can be generated. The amount of reactive power that can be generated is limited by the power rating of the power electronic converters and the amount of active power being exchanged between the converters (this active power is drawn from the network, and is not generated by the power electronic converters).

An HT can also be modelled using a Voltage Source Model (VSM) that includes a transformer, a series-connected voltage source and line impedance (Z^{HT}, which represents the impedance of the transformer's tertiary winding), and a shunt-connected voltage source and line impedance (Z^{sh}, which represents the impedance of the shunt connection coupling transformer) on the secondary side of the transformer, as shown in Figure 2.

The HT VSM can be converted into a Power Injection Model (PIM), where the control capabilities of the HT (volt/VAR control) are modelled with controlled power injections (shown in Figure 3). The equations that define the HT PIM are shown in (1)-(15). Formulae (1)-(4) define the compensating voltage provided by the HT, and (5)-(9), (11)-(12), and (14)-(15) define the power injections that simulate

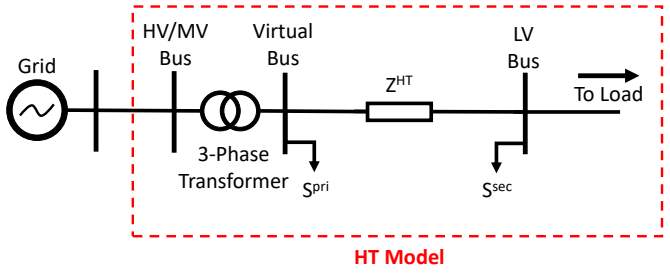

Fig. 3: Single line diagram of the HT PIM.

the compensation provided by the HT for a steady-state power flow simulation. Formulae (10) and (13) define the reactive power in the series converter.

$$-0.1 \leq r_{ij,\phi} \leq 0.1, \tag{1}$$

$$-\pi \leq \gamma_{ij,\phi} \leq \pi, \tag{2}$$

$$e^{pq}_{ij,\phi} = Re(r_{ij,\phi} v_{i,\phi} exp(-j\gamma_{ij,\phi})), \tag{3}$$

$$f^{pq}_{ij,\phi} = Im(r_{ij,\phi} v_{i,\phi} exp(-j\gamma_{ij,\phi})), \tag{4}$$

$$\begin{aligned} P^{pri}_{ij,\phi} &= G_{ij,\phi\phi}(-e_{i,\phi}e^{pq}_{ij,\phi} - f_{i,\phi}f^{pq}_{ij,\phi}) \\ &\quad + B_{ij,\phi\phi}(e_{i,\phi}f^{pq}_{ij,\phi} - f_{i,\phi}e^{pq}_{ij,\phi}), \end{aligned} \tag{5}$$

$$\begin{aligned} Q^{pri}_{ij,\phi} &= G_{ij,\phi\phi}(e_{i,\phi}f^{pq}_{ij,\phi} - f_{i,\phi}e^{pq}_{ij,\phi}) \\ &\quad + B_{ij,\phi\phi}(e_{i,\phi}e^{pq}_{ij,\phi} + f_{i,\phi}f^{pq}_{ij,\phi}), \end{aligned} \tag{6}$$

$$\begin{aligned} P^{se}_{ij,\phi} &= G_{ij,\phi\phi}(e_{j,\phi}e^{pq}_{ij,\phi} + f_{j,\phi}f^{pq}_{ij,\phi}) \\ &\quad + B_{ij,\phi\phi}(f_{j,\phi}e^{pq}_{ij,\phi} - e_{j,\phi}f^{pq}_{ij,\phi}), \end{aligned} \tag{7}$$

$$\begin{aligned} Q^{se}_{ij,\phi} &= G_{ij,\phi\phi}(f_{j,\phi}e^{pq}_{ij,\phi} - e_{j,\phi}f^{pq}_{ij,\phi}) \\ &\quad - B_{ij,\phi\phi}(e_{j,\phi}e^{pq}_{ij,\phi} + f_{j,\phi}f^{pq}_{ij,\phi}), \end{aligned} \tag{8}$$

$$\begin{aligned} P^{sh}_{ij,\phi} &= G_{ij,\phi\phi}\Big(\left(e^{pq}_{ij,\phi}\right)^2 + \left(f^{pq}_{ij,\phi}\right)^2 \\ &\quad + e_{i,\phi}e^{pq}_{ij,\phi} - e_{j,\phi}e^{pq}_{ij,\phi} + f_{i,\phi}f^{pq}_{ij,\phi} \\ &\quad - f_{j,\phi}f^{pq}_{ij,\phi}\Big) + B_{ij,\phi\phi}(e_{i,\phi}f^{pq}_{ij,\phi} \\ &\quad - e_{j,\phi}f^{pq}_{ij,\phi} - f_{i,\phi}e^{pq}_{ij,\phi} + f_{j,\phi}e^{pq}_{ij,\phi}), \end{aligned} \tag{9}$$

$$\begin{aligned} Q^{c}_{ij,\phi} &= G_{ij,\phi\phi}(e_{i,\phi}f^{pq}_{ij,\phi} - e_{j,\phi}f^{pq}_{ij,\phi} - f_{i,\phi}e^{pq}_{ij,\phi} \\ &\quad + f_{j,\phi}e^{pq}_{ij,\phi}) - B_{ij,\phi\phi}\Big(\left(e^{pq}_{ij,\phi}\right)^2 \\ &\quad + \left(f^{pq}_{ij,\phi}\right)^2 + e_{i,\phi}e^{pq}_{ij,\phi} - e_{j,\phi}e^{pq}_{ij,\phi} \\ &\quad + f_{i,\phi}f^{pq}_{ij,\phi} - f_{j,\phi}f^{pq}_{ij,\phi}\Big), \end{aligned} \tag{10}$$

$$|\overline{Q}_{ij,\phi}| = \left(\left(\overline{S}_{ij,\phi}\right)^2 - \left(P^{sh}_{ij,\phi}\right)^2\right)^{\frac{1}{2}}, \tag{11}$$

$$-|\overline{Q}_{ij,\phi}| \leq Q^{sh}_{ij,\phi} \leq |\overline{Q}_{ij,\phi}|, \tag{12}$$

$$-|\overline{Q}_{ij,\phi}| \leq Q^{c}_{ij,\phi} \leq |\overline{Q}_{ij,\phi}|, \tag{13}$$

$$P^{sec}_{ij,\phi} = P^{se}_{ij,\phi} - P^{sh}_{ij,\phi}, \tag{14}$$

$$Q^{sec}_{ij,\phi} = Q^{se}_{ij,\phi} + Q^{sh}_{ij,\phi}. \tag{15}$$

HT PIM formulae (5)-(10) can also be combined and rewritten to provide $S^{pri}_{ij,\phi}$, $S^{se}_{ij,\phi}$, and $S^{c}_{ij,\phi}$, which are the HT power injections $P^{pri}_{ij,\phi}$, $Q^{pri}_{ij,\phi}$, $P^{se}_{ij,\phi}$, $Q^{se}_{ij,\phi}$, and $P^{sh}_{ij,\phi}$ and the HT series converter reactive power, $Q^{c}_{ij,\phi}$, in the form of apparent power, as shown in (16)-(19).

$$v^{pq}_{ij,\phi} = e^{pq}_{ij,\phi} + jf^{pq}_{ij,\phi} \tag{16}$$

$$S^{pri}_{ij,\phi} = P^{pri}_{ij,\phi} + jQ^{pri}_{ij,\phi} = v_{i,\phi}\left(\frac{-v^{pq}_{ij,\phi}}{Z^{HT}_{ij,\phi\phi}}\right)^* \tag{17}$$

$$S^{se}_{ij,\phi} = P^{se}_{ij,\phi} + jQ^{se}_{ij,\phi} = v_{j,\phi}\left(\frac{v^{pq}_{ij,\phi}}{Z^{HT}_{ij,\phi\phi}}\right)^* \tag{18}$$

$$\begin{aligned} S^{c}_{ij,\phi} &= \sqrt{\left(P^{sh}_{ij,\phi}\right)^2 + \left(Q^{c}_{ij,\phi}\right)^2} \\ &= \left| v^{pq}_{ij,\phi}\left(\frac{v_{i,\phi} + v^{pq}_{ij,\phi} - v_{j,\phi}}{Z^{HT}_{ij,\phi\phi}}\right)^* \right| \end{aligned} \tag{19}$$

Regarding HT PIM formulae (1)-(4), it is possible to fully model the voltage compensation capability of the HT even if $r_{ij,\phi}$ is only permitted to have positive values due to the range used for $\gamma_{ij,\phi}$ ($-\pi$ to π). Negative HT compensating voltage could be achieved with a positive $r_{ij,\phi}$ value by phase shifting the compensating voltage enough to become negative. However, allowing $r_{ij,\phi}$ to have negative values does not misrepresent the capabilities of the HT. In the constraints of the LP used for the HT SLP additional restrictions are applied to $r_{ij,\phi}$ and $\gamma_{ij,\phi}$ to help mitigate inaccuracies, as described in Section III. With these additional restrictions applied, it may not be possible for the HT SLP to achieve negative HT voltage compensation if $r_{ij,\phi}$ is only permitted to be positive. This is because these additional restrictions could prevent the HT SLP from producing the phase angle required to achieve negative HT voltage compensation. In this case, HTs may not be optimally utilised by the HT SLP. Adjusting the additional restrictions to be more lenient is not a good solution in preventing such issues, as this could lead to more significant inaccuracies in HT SLP results. As such, $r_{ij,\phi}$ is permitted to have negative values, in order to help ensure that HTs are properly utilised by the HT SLP.

It should be noted that G_{ij} and B_{ij} correspond to Z^{HT} (i.e., $Z^{HT}=(G_{ij}+jB_{ij})^{-1}$). It should also be noted that HT line ij is modelled as having no mutual impedances, so G_{ij} and B_{ij} are diagonal matrices. This has been done because the inclusion of mutual impedances would result in the power injections made at one phase affecting the voltages at the other two phases, which is not accurate to the independent phase voltage control capability of HTs.

It should be noted that the power injections P^{se}_{ij} and Q^{se}_{ij} are impacted by P^{sh}_{ij} and Q^{sh}_{ij} due the shunt converter connecting at the HT LV bus (as shown in Figures 1 and 2). This results in the overall power injections at the HT LV bus, P^{sec}_{ij} and Q^{sec}_{ij}, as shown in (14) and (15). Additionally, the inclusion of P^{sh}_{ij} helps to ensure that no active power is generated by the HT PIM. However, the reactive power provided by the series converter, Q^{c}_{ij}, is not included in the power balance of Q^{sec}_{ij} or Q^{pri}_{ij}. This is because the impact of the series converter's compensating voltage is already fully modelled through the power injections P^{pri}_{ij}, Q^{pri}_{ij}, P^{se}_{ij}, Q^{se}_{ij}, and P^{sh}_{ij}. Instead,

Q^c_{ij} is used to track whether the reactive power provided by the series converter is feasible (i.e., does not exceed $|\overline{Q}_{ij}|$).

Power losses in the HT power electronics are modelled in the HT PIM through Z^{HT}. This is reflected in the power injections P^{pri}_{ij} and P^{sec}_{ij}, where the negative power injection will be larger than the positive power injection, resulting in an overall negative active power injection to represent the active power losses in the series-connected power converter. Whether P^{pri}_{ij} or P^{sec}_{ij} is negative is dependent on the voltage compensation provided, Z^{HT}, and network voltage levels. However, if Z^{HT} is assumed to be purely reactive $\left(R_{ij} = 0 \text{ and } G_{ij} = R_{ij}\left(R^2_{ij} + X^2_{ij}\right)^{-1} = 0\right)$, then the HT is modelled as having no active power losses in the power electronic converters, as such $P^{pri}_{ij,\phi}$ and $P^{sec}_{ij,\phi}$ sum together to equate zero, since no active power is being generated or lost.

It should also be noted that (5)-(15) and (17)-(19) are derived from the Unified Power Flow Controller (UPFC) PIM [23], [24]. UPFC PIM formulae was used to help model the HT due to the similarities between UPFCs and HTs. Both utilise series-connected and shunt-connected power electronic converters to provide voltage and reactive power compensation [2], [23], [24]. As such, due to these similarities, the PIM formulae used to model UPFC voltage and reactive power compensation are also applicable to HTs. The main difference between the HT PIM and UPFC PIM is that for the HT PIM the three phases are modelled separately, accommodating unbalanced power flow conditions, whereas the UPFC PIM generally assumes balanced power flow conditions. Adapting UPFC PIM formulae for modelling HTs in steady-state power flow simulation has been proven valid, as demonstrated in Section IV with Figures 8 and 9, where HT compensation is shown to have the intended impact on network voltage levels.

The three-phase transformer of the HT model is a passive component, and does not actively contribute to the voltage and/or reactive power compensation capabilities of the HT. The three-phase transformer is modelled with a nodal admittance matrix, which is defined by the transformer's per phase leakage admittance and winding configuration [25]. For the HT presented in this paper, the three-phase transformer has a wye-g/wye-g winding configuration. The nodal admittance matrix modelling method allows the three-phase transformer to be treated as a transmission line, and is accounted for in the network model by contributing to the network admittance matrix (applicable to the linear network model and Z-bus power flow simulation method utilised by the SLP [26], [27], [28], [29]). Power losses in the three-phase transformer are accounted for in this method. The nodal admittance matrix for a wye-g/wye-g winding configuration is defined in (20) and (21).

$$\overline{Y}_{Node} = \begin{bmatrix} \overline{Y}_I & -\overline{Y}_I \\ -\overline{Y}_I & \overline{Y}_I \end{bmatrix} \tag{20}$$

$$\overline{Y}_I = \begin{bmatrix} y_t & 0 & 0 \\ 0 & y_t & 0 \\ 0 & 0 & y_t \end{bmatrix} \tag{21}$$

III. SEQUENTIAL LINEAR PROGRAMMING METHOD.

This section proposes the HT SLP method, which maximises DG output by utilising HT PIMs.

SLP can be used to solve NLP problems by approximating them with a sequence of LP problems which are then solved in an iterative loop. Each successfully solved LP in the sequence brings the final output of the SLP closer to what the output of the NLP would be. Restrictions are applied to approximated LP constraints, typically in the form of step-size limits, to limit how far LPs can deviate from their initialisation points and minimise any potential inaccuracies. The results of an LP problem determine if restrictions need to be tightened in the event of inaccuracy, and how initialisation points are updated for the next iteration of the SLP loop. Typically, the SLP loop will continue until either a local optimal solution is found or some other termination condition (e.g., exceeding the maximum number of iterations) is met. What is considered a local optimal solution and how it is determined depends on the objective function and constraints of the original NLP problem.

The HT SLP method proposed here in this section is partially based on the SLP method described in [30]. Similar to the SLP method described in [30], the HT-SLP method utilises the linear network models from [26] and [27] as part of its OPF, uses nonlinear power flow simulation results to determine the accuracy of OPF results and to calculate OPF inputs, and requires that the initial nonlinear power flow simulation performed at the start of the SLP feature no voltage violations. The SLP method described in [30] uses an approximated euclidean distance constraint to restrict controllable loads in the OPF. However, the approximated euclidean distance constraint is only compatible with networks where all buses are 3-phase (limiting the network models that the SLP can work with), and prevents HT PIMs from being utilised (making it unsuitable for the HT SLP). As such, the HT SLP method instead uses step-size limits to restrict controllable loads (in this case HT PIMs and DG units) for its OPF method.

A. HT OPF.

As part of the proposed HT SLP method an OPF method was developed, referred to as the HT OPF. The objective for HT OPF method is to maximise the amount of DG power in a network while preventing voltage violations. The HT OPF method is an LP problem so that it can be integrated into the

HT SLP. The HT OPF method works under the assumptions that the networks are 3-phase, and that reverse power flow is acceptable. Furthermore, for the HT OPF method, the network model that is inputted into the OPF must feature no voltage violations before attempting to solve the HT OPF, otherwise, it cannot be guaranteed that a feasible solution will be found.

The HT PIM formulae (3)-(11) would cause the HT OPF to be nonlinear if it is implemented as it is. Therefore, in order for the HT OPF to be linear, First Order Taylor Series approximation is used to linearize (3)-(11) to produce the linear HT model constraints (22.39)-(22.47). Furthermore, step-size limits are applied to (1)-(2) and DG power outputs in order to restrict how far the controllable power injections, and by extension the network load profile, can deviate from their nominal operating points. The HT OPF is shown below.

$$\max \sum_{i\in\mathcal{N}^{DG}}\sum_{\phi\in\Omega} P_{i,\phi}^{DG} - w_1 \sum_{ij\in\varepsilon^{HT}}\sum_{\phi\in\Omega}(e_{ij,\phi}^{abs}+f_{ij,\phi}^{abs}) - w_2 \sum_{ij\in\varepsilon^{HT}}\sum_{\phi\in\Omega} Q_{ij,\phi}^{abs} \tag{22.1}$$

s.t.

$$e = Re\big(M^Y(x^Y+\Delta x^Y)s^{base} + M^\Delta(x^\Delta+\Delta x^\Delta)s^{base}+M^0\big)/v^{base}. \tag{22.2}$$

$$f = Im\big(M^Y(x^Y+\Delta x^Y)s^{base} + M^\Delta(x^\Delta+\Delta x^\Delta)s^{base}+M^0\big)/v^{base}. \tag{22.3}$$

$$|v| = \big(K^Y(x^Y+\Delta x^Y)s^{base} + K^\Delta(x^\Delta+\Delta x^\Delta)s^{base}+K^0\big)/v^{base}. \tag{22.4}$$

$$|\underline{v}| \le |v| \le |\overline{v}|. \tag{22.5}$$

$$\Delta x^\Delta = ((\Delta p^\Delta)^T,(\Delta q^\Delta)^T)^T. \tag{22.6}$$

$$\Delta p_{i,\phi}^\Delta = -P_{i,\phi}^{DG}, \tag{22.7}$$

$$\Delta q_{i,\phi}^\Delta = -Q_{i,\phi}^{DG}, \quad \forall i\in\mathcal{N}^{DG}\cap\mathcal{N}^\Delta,\ \forall\phi\in\Omega. \tag{22.8}$$

$$\Delta p_{i,\phi}^\Delta = 0, \tag{22.9}$$

$$\Delta q_{i,\phi}^\Delta = 0, \forall i\in\mathcal{N}^\Delta\backslash\mathcal{N}^{DG},\ \forall\phi\in\Omega. \tag{22.10}$$

$$\Delta x^Y = ((\Delta p^Y)^T,(\Delta q^Y)^T)^T. \tag{22.11}$$

$$\Delta p_{i,\phi}^Y = -P_{i,\phi}^{DG}, \tag{22.12}$$

$$\Delta q_{i,\phi}^Y = -Q_{i,\phi}^{DG}, \forall i\in\mathcal{N}^{DG}\cap\mathcal{N}^Y,\ \forall\phi\in\Omega. \tag{22.13}$$

$$\Delta p_{i,\phi}^Y = 0, \tag{22.14}$$

$$\Delta q_{i,\phi}^Y = 0, \quad \forall i\in\mathcal{N}^Y\backslash(\mathcal{N}^{HTp}\cup\mathcal{N}^{HTs}\cup\mathcal{N}^{DG}),\ \forall\phi\in\Omega. \tag{22.15}$$

$$P_{i,\phi}^{DG} \le min(\overline{P}_i, P_{i,\phi}^{DG(k)}+stp_{i,\phi}^{DG}), \tag{22.16}$$

$$P_{i,\phi}^{DG} \ge max(0, P_{i,\phi}^{DG(k)}-stp_{i,\phi}^{DG}), \tag{22.17}$$

$$Q_{i,\phi}^{DG} = P_{i,\phi}^{DG}\frac{\sqrt{1-PF_i^2}}{PF_i}, \quad \forall i\in\mathcal{N}^{DG},\ \forall\phi\in\Omega. \tag{22.18}$$

$$P_{i,0}^{DG} = P_{i,1}^{DG} = P_{i,2}^{DG}, \forall i\in\mathcal{N}^{DG}. \tag{22.19}$$

$$\Delta p_{i,\phi}^Y = -P_{ij,\phi}^{pri}, \tag{22.20}$$

$$\Delta p_{j,\phi}^Y = -P_{ij,\phi}^{sec}, \tag{22.21}$$

$$\Delta q_{i,\phi}^Y = -Q_{ij,\phi}^{pri}, \tag{22.22}$$

$$\Delta q_{j,\phi}^Y = -Q_{ij,\phi}^{sec}, \tag{22.23}$$

$$r_{ij,\phi} \le min(0.1, r_{ij,\phi}^{(k)}+stp^v), \tag{22.24}$$

$$r_{ij,\phi} \ge max(-0.1, r_{ij,\phi}^{(k)}-stp^v), \tag{22.25}$$

$$\gamma_{ij,\phi} \le min(\pi, \gamma_{ij,\phi}^{(k)}+stp^\gamma), \tag{22.26}$$

$$\gamma_{ij,\phi} \ge max(-\pi, \gamma_{ij,\phi}^{(k)}-stp^\gamma), \tag{22.27}$$

$$-|\overline{Q}_{ij,\phi}| \le Q_{ij,\phi}^{sh} \le |\overline{Q}_{ij,\phi}|, \tag{22.28}$$

$$Q_{ij,\phi}^{abs} \ge Q_{ij,\phi}^{sh}, \tag{22.29}$$

$$Q_{ij,\phi}^{abs} \ge -Q_{ij,\phi}^{sh}, \tag{22.30}$$

$$-|\overline{Q}_{ij,\phi}| \le Q_{ij,\phi}^{c} \le |\overline{Q}_{ij,\phi}|, \tag{22.31}$$

$$P_{ij,\phi}^{sec} = P_{ij,\phi}^{se} - P_{ij,\phi}^{sh}, \tag{22.32}$$

$$-\overline{S}_{ij,\phi} \le P_{ij,\phi}^{sh} \le \overline{S}_{ij,\phi}, \tag{22.33}$$

$$Q_{ij,\phi}^{sec} = Q_{ij,\phi}^{se} + Q_{ij,\phi}^{sh}, \tag{22.34}$$

$$e_{ij,\phi}^{abs} \ge e_{ij,\phi}^{pq}, \tag{22.35}$$

$$e_{ij,\phi}^{abs} \ge -e_{ij,\phi}^{pq}, \tag{22.36}$$

$$f_{ij,\phi}^{abs} \ge f_{ij,\phi}^{pq}, \tag{22.37}$$

$$f_{ij,\phi}^{abs} \ge -f_{ij,\phi}^{pq}, \tag{22.38}$$

$$\begin{aligned} e_{ij,\phi}^{pq} = Re\big(&r_{ij,\phi}^{(k)}v_{i,\phi}^{(k)}exp(-j\gamma_{ij,\phi}^{(k)}) \\ &+ v_{i,\phi}^{(k)}exp(-j\gamma_{ij,\phi}^{(k)})(r_{ij,\phi}-r_{ij,\phi}^{(k)}) \\ &+ r_{ij,\phi}^{(k)}exp(-j\gamma_{ij,\phi}^{(k)})((e_{i,\phi} \\ &+ jf_{i,\phi}) - v_{i,\phi}^{(k)}) \\ &- jr_{ij,\phi}^{(k)}v_{i,\phi}^{(k)}exp(-j\gamma_{ij,\phi}^{(k)})(\gamma_{ij,\phi} \\ &- \gamma_{ij,\phi}^{(k)})\big), \end{aligned} \tag{22.39}$$

$$\begin{aligned} f_{ij,\phi}^{pq} = Im\big(&r_{ij,\phi}^{(k)}v_{i,\phi}^{(k)}exp(-j\gamma_{ij,\phi}^{(k)}) \\ &+ v_{i,\phi}^{(k)}exp(-j\gamma_{ij,\phi}^{(k)})(r_{ij,\phi}-r_{ij,\phi}^{(k)}) \\ &+ r_{ij,\phi}^{(k)}exp(-j\gamma_{ij,\phi}^{(k)})((e_{i,\phi} \\ &+ jf_{i,\phi}) - v_{i,\phi}^{(k)}) \\ &- jr_{ij,\phi}^{(k)}v_{i,\phi}^{(k)}exp(-j\gamma_{ij,\phi}^{(k)})(\gamma_{ij,\phi} \\ &- \gamma_{ij,\phi}^{(k)})\big), \end{aligned} \tag{22.40}$$

$$\begin{aligned} |\overline{Q}_{ij,\phi}| = C_1(&((\overline{S}_{ij,\phi})^2-(P_{ij,\phi}^{sh(k)})^2)^{\frac{1}{2}} \\ &- (P_{ij,\phi}^{sh(k)}((\overline{S}_{ij,\phi})^2 \\ &- (P_{ij,\phi}^{sh(k)})^2)^{-\frac{1}{2}}(P_{ij,\phi}^{sh}-P_{ij,\phi}^{sh(k)}))), \end{aligned} \tag{22.41}$$

$$
\begin{aligned}
P^{pri}_{ij,\phi} = G_{ij,\phi\phi}\big(&-(e^{pq(k)}_{ij,\phi}e_{i,\phi} \\
&+ e^{(k)}_{i,\phi}e^{pq}_{ij,\phi} - e^{(k)}_{i,\phi}e^{pq(k)}_{ij,\phi}) \\
&- (f^{pq(k)}_{ij,\phi}f_{i,\phi} + f^{(k)}_{i,\phi}f^{pq}_{ij,\phi} \\
&- f^{(k)}_{i,\phi}f^{pq(k)}_{ij,\phi})\big) \\
&+ B_{ij,\phi\phi}\big((f^{pq(k)}_{ij,\phi}e_{i,\phi} \\
&+ e^{(k)}_{i,\phi}f^{pq}_{ij,\phi} - e^{(k)}_{i,\phi}f^{pq(k)}_{ij,\phi}) \\
&- (e^{pq(k)}_{ij,\phi}f_{i,\phi} + f^{(k)}_{i,\phi}e^{pq}_{ij,\phi} \\
&- f^{(k)}_{i,\phi}e^{pq(k)}_{ij,\phi})\big),
\end{aligned} \tag{22.42}
$$

$$
\begin{aligned}
Q^{pri}_{ij,\phi} = G_{ij,\phi\phi}\big(&(f^{pq(k)}_{ij,\phi}e_{i,\phi} \\
&+ e^{(k)}_{i,\phi}f^{pq}_{ij,\phi} - e^{(k)}_{i,\phi}f^{pq(k)}_{ij,\phi}) \\
&- (e^{pq(k)}_{ij,\phi}f_{i,\phi} + f^{(k)}_{i,\phi}e^{pq}_{ij,\phi} \\
&- f^{(k)}_{i,\phi}e^{pq(k)}_{ij,\phi})\big) \\
&+ B_{ij,\phi\phi}\big((e^{pq(k)}_{ij,\phi}e_{i,\phi} \\
&+ e^{(k)}_{i,\phi}e^{pq}_{ij,\phi} - e^{(k)}_{i,\phi}e^{pq(k)}_{ij,\phi}) \\
&+ (f^{pq(k)}_{ij,\phi}f_{i,\phi} + f^{(k)}_{i,\phi}f^{pq}_{ij,\phi} \\
&- f^{(k)}_{i,\phi}f^{pq(k)}_{ij,\phi})\big),
\end{aligned} \tag{22.43}
$$

$$
\begin{aligned}
P^{se}_{ij,\phi} = G_{ij,\phi\phi}\big(&(e^{pq(k)}_{ij,\phi}e_{j,\phi} \\
&+ e^{(k)}_{j,\phi}e^{pq}_{ij,\phi} - e^{(k)}_{j,\phi}e^{pq(k)}_{ij,\phi}) \\
&+ (f^{pq(k)}_{ij,\phi}f_{j,\phi} + f^{(k)}_{j,\phi}f^{pq}_{ij,\phi} \\
&- f^{(k)}_{j,\phi}f^{pq(k)}_{ij,\phi})\big) \\
&+ B_{ij,\phi\phi}\big((e^{pq(k)}_{ij,\phi}f_{j,\phi} \\
&+ f^{(k)}_{j,\phi}e^{pq}_{ij,\phi} - f^{(k)}_{j,\phi}e^{pq(k)}_{ij,\phi}) \\
&- (f^{pq(k)}_{ij,\phi}e_{j,\phi} + e^{(k)}_{j,\phi}f^{pq}_{ij,\phi} \\
&- e^{(k)}_{j,\phi}f^{pq(k)}_{ij,\phi})\big),
\end{aligned} \tag{22.44}
$$

$$
\begin{aligned}
Q^{se}_{ij,\phi} = G_{ij,\phi\phi}\big(&(e^{pq(k)}_{ij,\phi}f_{j,\phi} \\
&+ f^{(k)}_{j,\phi}e^{pq}_{ij,\phi} - f^{(k)}_{j,\phi}e^{pq(k)}_{ij,\phi}) \\
&- (f^{pq(k)}_{ij,\phi}e_{j,\phi} + e^{(k)}_{j,\phi}f^{pq}_{ij,\phi} \\
&- e^{(k)}_{j,\phi}f^{pq(k)}_{ij,\phi})\big) \\
&- B_{ij,\phi\phi}\big(e^{pq(k)}_{ij,\phi}e_{j,\phi} \\
&+ e^{(k)}_{j,\phi}e^{pq}_{ij,\phi} - e^{(k)}_{j,\phi}e^{pq(k)}_{ij,\phi}) \\
&+ (f^{pq(k)}_{ij,\phi}f_{j,\phi} + f^{(k)}_{i,\phi}f^{pq}_{ij,\phi} \\
&- f^{(k)}_{j,\phi}f^{pq(k)}_{ij,\phi})\big),
\end{aligned} \tag{22.45}
$$

$$
\begin{aligned}
P^{sh}_{ij,\phi} = G_{ij,\phi\phi}\big(&(-\left(e^{pq(k)}_{ij,\phi}\right)^2 - \left(f^{pq(k)}_{ij,\phi}\right)^2 \\
&+ 2e^{pq}_{ij,\phi}e^{pq(k)}_{ij,\phi} + 2f^{pq}_{ij,\phi}f^{pq(k)}_{ij,\phi}) \\
&+ (e^{pq(k)}_{ij,\phi}e_{i,\phi} + e^{(k)}_{i,\phi}e^{pq}_{ij,\phi} \\
&- e^{(k)}_{i,\phi}e^{pq(k)}_{ij,\phi}) - (e^{pq(k)}_{ij,\phi}e_{j,\phi} \\
&+ e^{(k)}_{j,\phi}e^{pq}_{ij,\phi} - e^{(k)}_{j,\phi}e^{pq(k)}_{ij,\phi}) \\
&+ (f^{pq(k)}_{ij,\phi}f_{i,\phi} + f^{(k)}_{i,\phi}f^{pq}_{ij,\phi} \\
&- f^{(k)}_{i,\phi}f^{pq(k)}_{ij,\phi}) - (f^{pq(k)}_{ij,\phi}f_{j,\phi} \\
&+ f^{(k)}_{j,\phi}f^{pq}_{ij,\phi} - f^{(k)}_{j,\phi}f^{pq(k)}_{ij,\phi})\big) \\
&+ B_{ij,\phi\phi}\big((f^{pq(k)}_{ij,\phi}e_{i,\phi} + e^{(k)}_{i,\phi}f^{pq}_{ij,\phi} \\
&- e^{(k)}_{i,\phi}f^{pq(k)}_{ij,\phi}) - (f^{pq(k)}_{ij,\phi}e_{j,\phi} \\
&+ e^{(k)}_{j,\phi}f^{pq}_{ij,\phi} - e^{(k)}_{j,\phi}f^{pq(k)}_{ij,\phi}) \\
&- (e^{pq(k)}_{ij,\phi}f_{i,\phi} + f^{(k)}_{i,\phi}e^{pq}_{ij,\phi} \\
&- f^{(k)}_{i,\phi}e^{pq(k)}_{ij,\phi}) + (e^{pq(k)}_{ij,\phi}f_{j,\phi} \\
&+ f^{(k)}_{j,\phi}e^{pq}_{ij,\phi} - f^{(k)}_{j,\phi}e^{pq(k)}_{ij,\phi})\big),
\end{aligned} \tag{22.46}
$$

$$
\begin{aligned}
Q^{c}_{ij,\phi} = G_{ij,\phi\phi}\big(&(f^{pq(k)}_{ij,\phi}e_{i,\phi} + e^{(k)}_{i,\phi}f^{pq}_{ij,\phi} \\
&- e^{(k)}_{i,\phi}f^{pq(k)}_{ij,\phi}) - (f^{pq(k)}_{ij,\phi}e_{j,\phi} \\
&+ e^{(k)}_{j,\phi}f^{pq}_{ij,\phi} - e^{(k)}_{j,\phi}f^{pq(k)}_{ij,\phi}) \\
&- (e^{pq(k)}_{ij,\phi}f_{i,\phi} + f^{(k)}_{i,\phi}e^{pq}_{ij,\phi} \\
&- f^{(k)}_{i,\phi}e^{pq(k)}_{ij,\phi}) + (e^{pq(k)}_{ij,\phi}f_{j,\phi} \\
&+ f^{(k)}_{j,\phi}e^{pq}_{ij,\phi} - f^{(k)}_{j,\phi}e^{pq(k)}_{ij,\phi})\big) \\
&- B_{ij,\phi\phi}\big((-\left(e^{pq(k)}_{ij,\phi}\right)^2 - \left(f^{pq(k)}_{ij,\phi}\right)^2 \\
&+ 2e^{pq}_{ij,\phi}e^{pq(k)}_{ij,\phi} + 2f^{pq}_{ij,\phi}f^{pq(k)}_{ij,\phi}) \\
&+ (e^{pq(k)}_{ij,\phi}e_{i,\phi} + e^{(k)}_{i,\phi}e^{pq}_{ij,\phi} \\
&- e^{(k)}_{i,\phi}e^{pq(k)}_{ij,\phi}) - (e^{pq(k)}_{ij,\phi}e_{j,\phi} \\
&+ e^{(k)}_{j,\phi}e^{pq}_{ij,\phi} - e^{(k)}_{j,\phi}e^{pq(k)}_{ij,\phi}) \\
&+ (f^{pq(k)}_{ij,\phi}f_{i,\phi} + f^{(k)}_{i,\phi}f^{pq}_{ij,\phi} \\
&- f^{(k)}_{i,\phi}f^{pq(k)}_{ij,\phi}) - (f^{pq(k)}_{ij,\phi}f_{j,\phi} \\
&+ f^{(k)}_{j,\phi}f^{pq}_{ij,\phi} - f^{(k)}_{j,\phi}f^{pq(k)}_{ij,\phi})\big), \\
&\forall (i,j) \in \varepsilon^{HT},\ \forall \phi \in \Omega.
\end{aligned} \tag{22.47}
$$

The objective function of the HT OPF, (22.1), is to maximise the sum of DG unit active power outputs while minimising HT compensation (with weighting being used to prioritise the main objective of maximising DG unit power output). The overall goal of the HT OPF is to maximise DG active power output (reactive power output is not considered since only active power is considered useful in most cases) as much as possible by utilising HT voltage and reactive power compensation capabilities to prevent any network constraint violations that may occur as a result of increasing DG active power output (such as voltage violations). HT compensation is minimised in (22.1) to prevent the HT OPF from utilising HT PIMs excessively or when they are not required. This helps to prevent premature termination of the HT SLP since premature

use of HT capabilities can result in failed HT accuracy checks, which results in step-size restrictions being tightened, which can lead to termination (as shown later in this section). Premature termination of the SLP can result in DG outputs that do not properly represent the potential benefits of HT utilisation. The inclusion of the weighted sums in (22.1) does not disrupt the main objective of maximising DG output, the OPF will maximise DG output within the boundaries of the given constraints, provided that appropriate values are selected for the weights. Since the HT OPF's objective to maximise DG active power output is not disrupted by the inclusion of the weighted sums, then the HT SLP's ability to reach a local optimal solution will also not be disrupted, provided that HT OPF results are accurate. The values of the weights depend on the size of the DGs, base apparent power, network voltage levels, base voltage, and HT power ratings. As such, the values for weights will differ on a case-by-case basis, however, as a general rule, the values for the weights should scale the values of $\sum_{ij\in\varepsilon^{HT}}\sum_{\phi\in\Omega}(e^{abs}_{ij,\phi}+f^{abs}_{ij,\phi})$ and $\sum_{ij\in\varepsilon^{HT}}\sum_{\phi\in\Omega}Q^{abs}_{ij,\phi}$ such that they are between four to six orders of magnitude smaller than $\sum_{i\in\mathcal{N}^{DG}}\sum_{\phi\in\Omega}P^{DG}_{i,\phi}$ for all SLP iterations where HT compensation is utilised. Such values will encourage the OPF to utilise HT compensation only when it is necessary to prevent voltage violations, and prevent unnecessary use of HTs. If inappropriate values are selected for weights, then HT compensation may be excessive and premature (which can lead to premature termination of the SLP, as previously stated), or HT compensation may not be fully utilised (which can reduce the amount of additional DG output that can be achieved).

It should be noted that the linear multi-phase network model matrices used to model how changes to network loads impact network voltages, M^Y, M^Δ, M^0, K^Y, K^Δ, and K^0, are described in detail in [26] and [27].

Equations (22.2) and (22.3) are the constraints for the real and imaginary parts of the network voltages, (22.4) is the constraint for the network voltage magnitudes, and (22.5) is the constraint for the upper and lower network voltage limits. Equations (22.6)-(22.15) and (22.20)-(22.23) are the constraints that define how P^{DG} and the HT power injections are used to create the power injection vectors Δx^Δ and Δx^Y. Inequalities (22.16) and (22.17) define the maximum and minimum outputs for DG units, (22.18) defines DG reactive power output, and (22.19) ensures that the outputs for DG units are balanced. Inequalities (22.24)-(22.27) define the maximum and minimum values for r and γ. Equations (22.39) and (22.40) are the constraints that define the real and imaginary parts of the HT compensating voltage. Equations (22.42) and (22.43) define the HT power injections at the virtual bus. Equation (22.41) is the constraint that defines the maximum magnitude for the reactive power outputs for the shunt and series power electronic converters. Formulae (22.28), (22.32)-(22.34), and (22.44)-(22.46) define the HT power injections at the LV bus, with (22.33) ensuring that the active power exchange between the converters does not exceed the apparent power rating of the converters. Formulae (22.47) and (22.31) define the reactive power in the series converter due to the HT compensating voltage. Inequalities (22.29), (22.30), and (22.35)-(22.38) define the e^{abs}, f^{abs}, and Q^{abs} decision variables.

B. HT SLP Process.

A flowchart describing the process of the HT SLP method is shown in Figure 4. In Figure 4 it can be seen that the HT SLP involves a process of solving the HT OPF (using the nominal operating points and linear network model matrices as inputs), checking that HT OPF results are feasible and accurate, adjusting step-sizes, updating OPF inputs, and checking to see if a local optimum solution has been found.

At the start of every HT SLP iteration, the current iteration number, k, will be compared against the maximum allowable number of iterations, $\overline{k}$. If k exceeds $\overline{k}$, then the HT SLP will terminate and the HT OPF results of the previous iteration, $k-1$, will be taken as the closest the HT SLP will get to a local optimum solution. Otherwise, the HT SLP will continue onto the next step of the process.

The first set of nominal operating points and linear network model matrices are derived from a Z-bus power flow simulation [28], [29] where the HT models and DG units are inactive. From the results, $v^{(k)}$, $e^{(k)}$, $f^{(k)}$, and the linear network model matrices are derived, and nominal operating points relating to HT model and DG unit variables ($e^{pq\ (k)}$, $f^{pq\ (k)}$, $r^{(k)}$, $\gamma^{(k)}$, $P^{sh(k)}$, and $P^{DG(k)}$) are set to zero. After HT OPF results are confirmed to be feasible and accurate, nominal operating points are updated using HT OPF results (e.g. $e^{pq(k+1)} \leftarrow e^{pq*}$ and $k \leftarrow (k+1)$, where e^{pq*} is the OPF output for the real part of the HT compensating voltages). Linear network model matrices are updated at the start of the next HT SLP iteration using the power flow results of the previous iteration. The updated nominal operating points and linear network model matrices then serve as the inputs for the next iteration's HT OPF.

HT OPF results go through two checks to determine whether they are feasible and accurate. First they are subjected to the 'Network Feasibility Check', where the updated power flow results are checked for any voltage violations. If there are voltage violations, then the DG and HT step-sizes are reduced by 50% and the HT OPF is rerun with the new step-sizes. Both DG and HT step-sizes are reduced because there can be instances where the HT OPF is applying the same amount of power from DG units as the previous iteration but utilising less compensation from the HT models which can lead to voltage violations (this is caused by e^{abs}_{ij}, f^{abs}_{ij}, and Q^{abs}_{ij} being minimised by the objective function). If there are no voltage violations, then the HT SLP proceeds onto the 'HT Accuracy Check', where it is determined whether the HT power injections provided by the HT OPF produce the correct compensating voltages, and to make sure that the apparent power through the series converter, $S^c_{ij} \in \mathbb{R}^\Omega$, does not exceed

$\overline{S}_{ij}$. The 'HT Accuracy Check' makes use of the HT PIM formulae (17)-(19) in order to determine the accuracy of the HT compensation power injections provided by the HT OPF, as seen in (23)-(24) and (28). The updated power flow results and HT OPF power injections are used to calculate the actual compensating voltages provided by HT models, as shown in (23)-(27).

$$v_{ij,\phi}^{pq1} = -Z_{ij,\phi\phi}^{HT}\left(\frac{S_{ij,\phi}^{pri}}{v_{i,\phi}}\right)^{*}, \tag{23}$$

$$v_{ij,\phi}^{pq2} = Z_{ij,\phi\phi}^{HT}\left(\frac{S_{ij,\phi}^{se}}{v_{j,\phi}}\right)^{*}, \tag{24}$$

$$v_{ij,\phi}^{pq\ act} = \frac{v_{ij,\phi}^{pq1} + v_{ij,\phi}^{pq2}}{2}, \tag{25}$$

$$\Delta v_{ij,\phi}^{pq} = |v_{ij,\phi}^{pq\ act} - v_{ij,\phi}^{pq\ OPF}|, \tag{26}$$

$$v_{ij}^{sum} = \sum_{\phi\epsilon\Omega}\Delta v_{ij,\phi}^{pq}, \tag{27}$$

$$\forall(i,j) \in \varepsilon^{HT},\ \forall\phi \in \Omega.$$

It should be noted that both $v_{ij,\phi}^{pq1}$ and $v_{ij,\phi}^{pq2}$ are attempts to calculate the HT compensating voltage. If there are no inaccuracies, then $v_{ij,\phi}^{pq1} = v_{ij,\phi}^{pq2}$. However, since $P_{ij,\phi}^{pri}$, $Q_{ij,\phi}^{pri}$, $P_{ij,\phi}^{se}$, and $Q_{ij,\phi}^{se}$ are calculated using linear approximations of (5)-(8), their values are not entirely accurate. Therefore, due to these minor inaccuracies, $v_{ij,\phi}^{pq1}$ and $v_{ij,\phi}^{pq2}$ can slightly differ from one another. Due to these slight differences, although unlikely, it is possible that using one value may result in a successful 'HT Accuracy Check', but using the other would result in a failed 'HT Accuracy Check'. As such, $v_{ij,\phi}^{pq\ act}$ is calculated by averaging $v_{ij,\phi}^{pq1}$ and $v_{ij,\phi}^{pq2}$ together. Therefore, in the event that the differences between $v_{ij,\phi}^{pq1}$ and $v_{ij,\phi}^{pq2}$ would lead to different results for the 'HT Accuracy Check', utilising $v_{ij,\phi}^{pq\ act}$ will help to provide a definitive answer to whether the 'HT Accuracy Check' is considered to have succeeded or failed.

The $v_{ij}^{pq\ act}$ values are then used to calculate S_{ij}^{c}:

$$S_{ij,\phi}^{c} = \left| v_{ij,\phi}^{pq\ act}\left(\frac{v_{i,\phi} + v_{ij}^{pq\ act} - v_{j,\phi}}{Z_{ij,\phi\phi}^{HT}}\right)^{*}\right|, \tag{28}$$

$$\forall(i,j) \in \varepsilon^{HT},\ \forall\phi \in \Omega.$$

All v_{ij}^{sum} values are then compared to a predetermined tolerance, $v^{tol} \in \mathbb{R}$, and all $S_{ij,\phi}^{c}$ values are compared to the appropriate $\overline{S}_{ij}$ values. If any v_{ij}^{sum} value exceeds v^{tol}, or if any $S_{ij,\phi}^{c}$ value exceeds its appropriate $\overline{S}_{ij}$ value, then the HT OPF results are considered to be inaccurate, HT step-sizes are reduced by 50%, and the HT OPF is rerun with the new step-size values. Otherwise, the HT OPF results are considered to be accurate.

If reduced, HT step-size stp^{v} is compared to a minimum tolerance value, $\underline{stp}^{v} \in \mathbb{R}$. If stp^{v} is less than $\underline{stp}^{v}$, then the HT SLP terminates and the results from the last feasible iteration are taken as the closest the HT SLP will get to a local optimum solution.

The final step of the HT SLP loop compares the $\sum_{i\in\mathcal{N}^{DG}}\sum_{\phi\in\Omega}P_{i,\phi}^{DG}$ of the current iteration (k) to the previous iteration ($k-1$). If the difference between the two values falls below a predetermined tolerance, $P^{tol} \in \mathbb{R}$, then the HT SLP terminates and takes the latest HT OPF results as the local optimum solution. Otherwise, the HT SLP loop starts again.

SLP is used to find local optimal solutions to nonlinear, non-convex optimisation problems by solving a sequence of LP problems. As such, there is no guarantee that a global optimal solution will be found by the optimisation solvers by the end of the SLP process. However, the local optimal solution found the HT SLP should serve as satisfactory demonstration of the potential benefit of implementing HTs into a distribution network. The solution quality of the final SLP results can be gauged by comparing the final $\sum_{i\in\mathcal{N}^{DG}}\sum_{\phi\in\Omega}P_{i,\phi}^{DG}$ output of the SLP to the maximum amount of $\sum_{i\in\mathcal{N}^{DG}}\sum_{\phi\in\Omega}P_{i,\phi}^{DG}$ output possible without HT implementation. If the final value of $\sum_{i\in\mathcal{N}^{DG}}\sum_{\phi\in\Omega}P_{i,\phi}^{DG}$ produced by the SLP noticeably exceeds the amount of $\sum_{i\in\mathcal{N}^{DG}}\sum_{\phi\in\Omega}P_{i,\phi}^{DG}$ possible without HT implementation, then this indicates that the SLP has successfully utilised HTs to maximise DG output. Furthermore, the final SLP results would have successfully passed the 'Network Feasibility Check' and the 'HT Accuracy Check', demonstrating that the results from the HT OPF were of a satisfactory level of accuracy. Which demonstrates that the final results of the SLP successfully utilised HTs to maximise DG output, and that the results are accurate to an appropriate level.

IV. RESULTS.

This section describes the test case networks used to determine the effectiveness of the proposed HT SLP method, and presents the results from said test cases, demonstrating that the HT SLP is capable of reducing the curtailment of DG output.

Sensitivity analysis is performed in both test cases, where different values for w_1 and w_2 are implemented to demonstrate the impact that the weight values can have on HT SLP results (e.g., premature SLP termination, HTs utilised beyond what is necessary, or HTs not being fully utilised).

Furthermore, as previously mentioned, an alternative SLP method was developed to maximise DG output without utilising HTs, referred to as the No-HT SLP. This was done so that the impact of HT utilisation could be more clearly demonstrated. Further details on the No-HT SLP method can be found in Appendix A.

For both test cases, Gurobi was used as the solver for the optimisation problems and Z-bus power flow simulations were performed in Python using OPEN (electrical power network simulation software in Python) [31]. The test cases

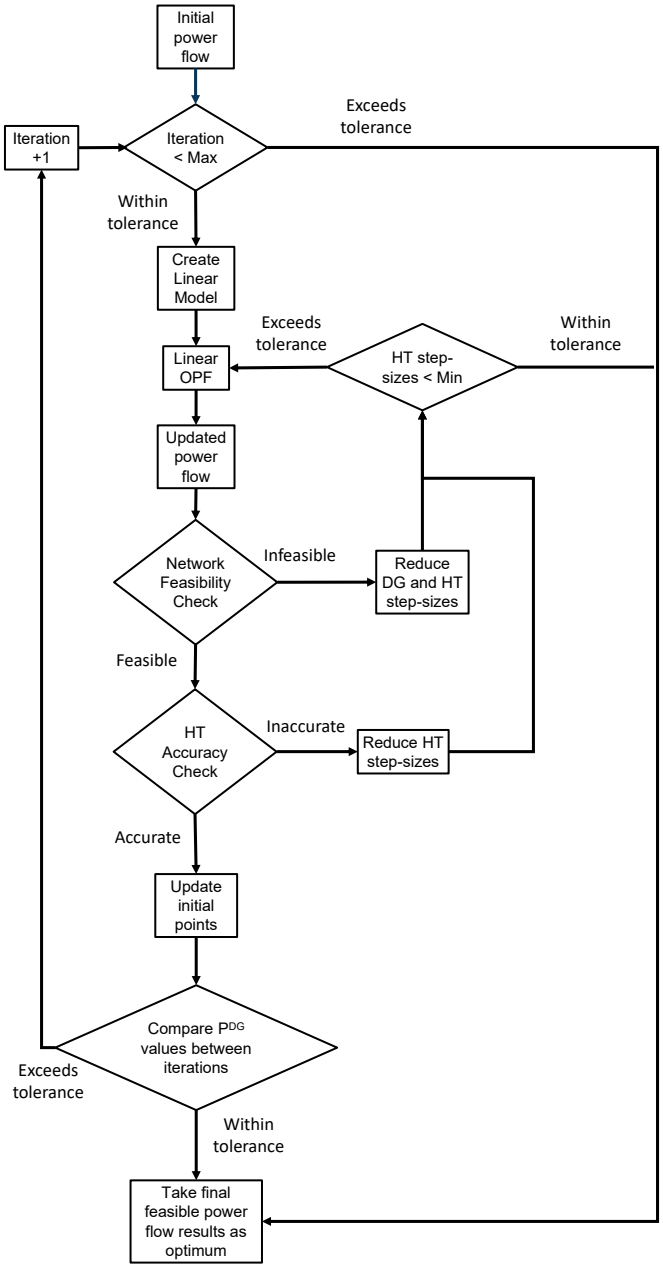

Fig. 4: The HT SLP Flowchart.

were run on an HP EliteBook with an Intel i7-10610u, and 32 GB of RAM.

It should be noted that for Tables V, VI, VIII, and IX, in the 'Termination' columns, 'Opt' refers to the SLP terminating after finding a local optimal solution (as described in Section III), and 'Stp' refers to the SLP terminating because $stp^v < \underline{stp^v}$.

A. 69-Bus System Test Case Setup.

A modified IEEE 69-Bus system [32] was used as the test case to determine whether the HT SLP method was capable of coordinating multiple HT models to achieve the given objective function. The 69-Bus system was selected as it was large enough to accommodate multiple HT models. The upper and lower voltage boundaries for the 69-Bus system are 1.1pu and 0.9pu respectively, as stated in [32]. For this test case, the HT models were capable of power factor correction through reactive power compensation and $\pm 10\%$ independent phase voltage control (i.e., $-0.1 \leq r_{ij} \leq 0.1$). For all HTs, the maximum power rating of the power electronic converters, $\overline{S}$, is $1/10^{th}$ of the transformer's power rating. Furthermore, for all HT models, Z^{HT} is $1/10^{th}$ of the transformer's equivalent impedance, and is purely reactive (HT converter active power loss is assumed to be negligible). Power losses in the HT power electronics are ignored, so that it was easier to ensure that none of the HT OPF outputs resulted in any HT PIMs generating any active power.

The modified IEEE 69-Bus system can be seen in Figure 5. In order to make the 69-Bus system unbalanced, the nominal load values were multiplied by factors of 1, 1.09 and 0.91 for phases A, B, and C respectively (similar to how the 69-Bus system was made unbalanced in [33]). The modifications made to the 69-Bus system also include adding 3 HT models, and replacing the loads at buses 27, 35, and 65 with DG units. The HT PIM parameters are shown in Table I, where R^{tf} and X^{tf} are the transformer's equivalent resistance and reactance, R^{HT} and X^{HT} are the resistance and reactance for the tertiary winding, $\overline{S}^{tf}$ is the transformer power rating, and $\overline{S}$ is the maximum power rating for the HT power electronic converters. R^{tf} and X^{tf} dictate R^{HT} and X^{HT} $\left(\text{i.e., } \sqrt{(R_{ij}^{tf})^2+(X_{ij}^{tf})^2}=10\sqrt{(R_{ij}^{HT})^2+(X_{ij}^{HT})^2}\right)$. R^{HT} and X^{HT} dictate Z^{HT} $\left(\text{i.e., } Z_{ij,\phi\phi}^{HT}=R_{ij}^{HT}+jX_{ij}^{HT}\right)$ and, by extension, B_{ij} and G_{ij} $\left(\text{i.e., } G_{ij,\phi\phi}=R_{ij}^{HT}\Big/\left(\left(R_{ij}^{HT}\right)^2+\left(X_{ij}^{HT}\right)^2\right)\right.$ and $\left.B_{ij,\phi\phi}=X_{ij}^{HT}\Big/\left(\left(R_{ij}^{HT}\right)^2+\left(X_{ij}^{HT}\right)^2\right)\right)$, which are used to calculate the HT compensation power injections P^{pri}, Q^{pri}, P^{se}, Q^{se}, P^{sh}, and Q^{c} as seen in (5)-(10). $\overline{S}$ is used to dictate the boundaries for P^{sh}, Q^{c}, and Q^{sh} as seen in (11)-(13) and (22.33) $\left(\text{i.e., } \overline{S}_{ij,\phi}\geq\sqrt{\left(P_{ij,\phi}^{sh}\right)^2+\left(Q_{ij,\phi}^{sh}\right)^2}\right.$ and $\left.\overline{S}_{ij,\phi}\geq\sqrt{\left(P_{ij,\phi}^{sh}\right)^2+\left(Q_{ij,\phi}^{c}\right)^2}\right)$. For DG 1 $\overline{P}=3$ MW, for DG 2, $\overline{P}=5$ MW, and for DG 3 $\overline{P}=3.5$ MW. Furthermore, it is assumed that all DG units operate at unity power factor, only outputting active power. Also, the inclusion of the HT model impedances result in bus voltage levels lowering and the initial power flow simulation of the network prior to the HT SLP loop having voltage violations. Therefore, all loads were multiplied by a factor of 0.75 in order to prevent voltage violations in the initial power flow simulation of the network (as required by the proposed SLP methods). The initial phase voltage levels of the modified network can be seen in Figure 6.

The values used for the HT OPF constants (excluding w_1 and w_2) for this test case are shown in Table II. The values utilised for w_1 and w_2 as part of the sensitivity analysis are: 0, 0.01, and 0.001.

B. European Low Voltage Test Feeder Test Case Setup

A modified version of the IEEE EULV test feeder [34] was also used as a test case for the HT SLP method. Similar to the 69-Bus system, the EULV test feeder was chosen as

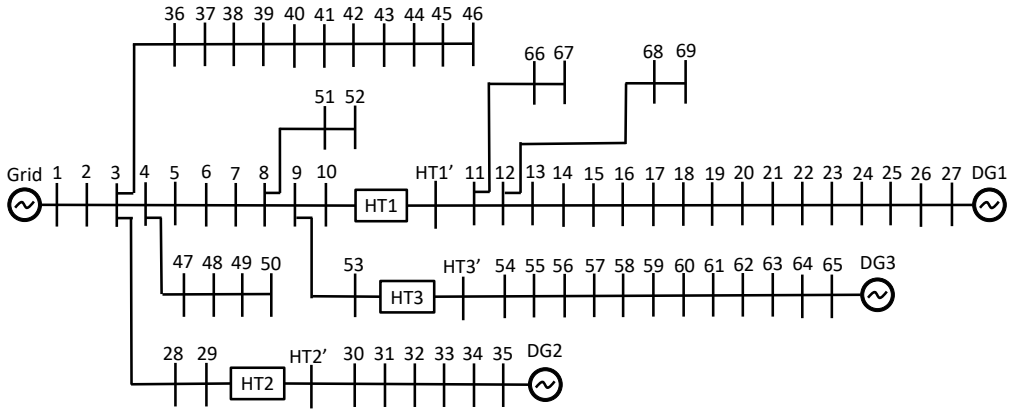

Fig. 5: The modified IEEE 69-Bus system, where HT1', HT2', and HT3' are the LV buses of the HT PIMs.

TABLE I: 69 Bus System HT PIM Parameters

	R^{tf} (Ω)	X^{tf} (Ω)	R^{HT} (Ω)	X^{HT} (Ω)	$\overline{S}^{tf}$ (MVA)	$\overline{S}$ (MVA)
HT 1	0.82	0.27	0	0.086	3	0.3
HT 2	0.06	0.16	0	0.017	5	0.5
HT 3	2.03	1.03	0	0.228	3.5	0.35

TABLE II: 69 Bus System HT OPF Constants

v^{tol}	0.0004 pu	P^{tol}	0.01 W
C_1	0.99	s^{base}	5000 MVA
stp^{v}	0.01	v^{base}	12.66 kV
stp^{γ}	0.01π	$\lvert\overline{v}\rvert$	1.1 pu
$\underline{stp^{v}}$	0.0001	$\lvert\underline{v}\rvert$	0.9 pu
stp_i^{DG}	$0.1\overline{P}_i \ \forall i \in \mathcal{N}^{DG}$		

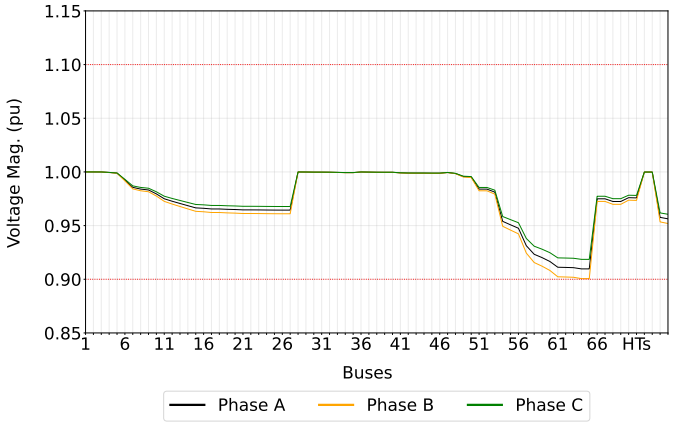

Fig. 6: The phase voltage magnitude levels of the initial 69-Bus system before HT or DG utilisation.

a test case as it was large enough to accommodate multiple HT models. The upper and lower voltage boundaries chosen for this test case are 1.1pu and 0.9pu, respectively. For this test case, the HT models were capable of reactive power compensation and $\pm 10\%$ independent phase voltage control. For all HTs, the maximum power rating the HT power electronic converters, $\overline{S}$, is $1/10^{th}$ of the transformer's power rating. Furthermore, for all HT models Z^{HT} is $1/10^{th}$ of the transformer's equivalent impedance, and is purely reactive (HT converter active power loss is assumed to be negligible). Again, power losses in the HT power electronics are ignored, so that it was easier to ensure that none of the HT OPF outputs resulted in any HT PIMs generating any active power.

TABLE III: Reduced EULV Test Feeder HT PIM Parameters

	R^{tf} (Ω)	X^{tf} (Ω)	R^{HT} (Ω)	X^{HT} (Ω)	$\overline{S}^{tf}$ (kVA)	$\overline{S}$ (kVA)
HT 1	0.064	0.006	0	0.006	40	4
HT 2	0.069	0.007	0	0.007	40	4
HT 3	0.132	0.020	0	0.013	40	4

The original EULV test feeder is comprised of 908 buses and 907 lines. However, many of the buses in the original network only serve to connect two lines together, and therefore, are redundant and can be removed. Therefore, a reduced version of the EULV test feeder (referred to as the Reduced EULV test feeder) has been used for this paper, where redundant buses have been removed, and the lines between them have been merged together. Without the HTs, the Reduced EULV test feeder is comprised of 125 buses, and 123 lines. All of the load buses and buses that act as junction points from the original EULV test feeder have been retained. The default EULV test feeder loads have been implemented in the Reduced EULV test feeder test case. The Reduced EULV test feeder has been further modified by the addition of 3 HTs and 2 DGs (placed at buses 604 and 839), as shown in Figure 7. With the HTs, the Reduced EULV test feeder is comprised of 131 buses, and 126 lines. HT parameters are shown in Table III. For DG 1, $\overline{P} = 35kW$, and for DG 2, $\overline{P} = 25kW$. Again, it is assumed that all DGs operate at unity power factor, only outputting active power.

The values used for the HT OPF constants (excluding w_1 and w_2) for this test case are shown in Table IV. The values utilised for w_1 and w_2 as part of the sensitivity analysis are: 0, 0.1, and 0.01.

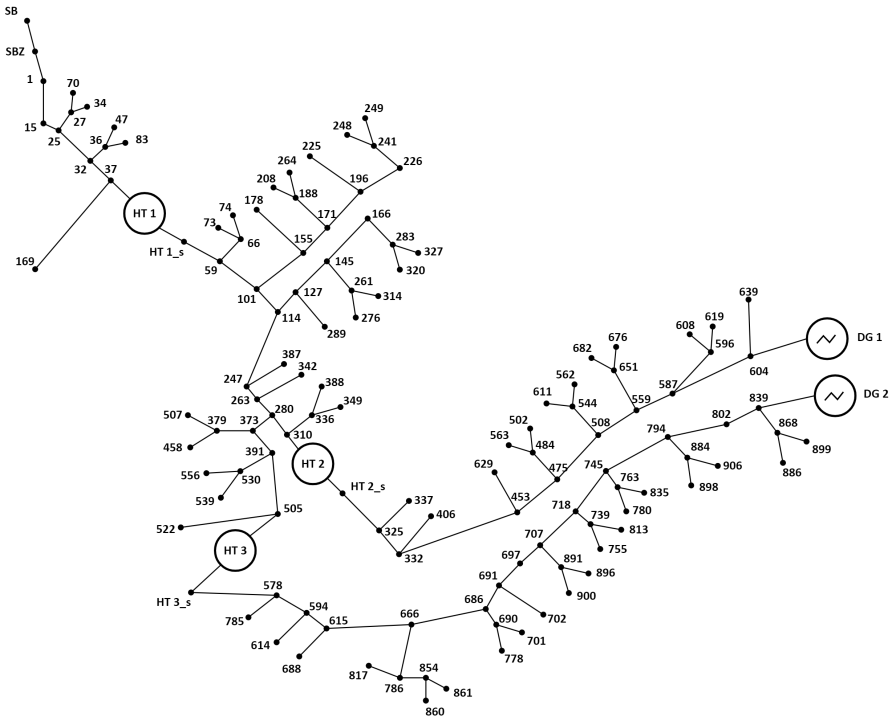

Fig. 7: Reduced EULV test feeder test case.

TABLE IV: Reduced EULV Test Feeder HT OPF Constants

v^{tol}	0.002 pu	P^{tol}	0.01 W
C_1	0.99	s^{base}	0.8 MVA
stp^{v}	0.01	v^{base}	240 V
stp^{γ}	0.01π	$\lvert\overline{v}\rvert$	1.1 pu
$\underline{stp}^{v}$	0.0001	$\lvert\underline{v}\rvert$	0.9 pu
stp_i^{DG}	$0.1\overline{P}_i \ \forall i \in \mathcal{N}^{DG}$		

TABLE V: 69-Bus System No-HT SLP Results

$\sum_{i\in\mathcal{N}^{DG}}\sum_{\phi\in\Omega} P_{i,\phi}^{DG}$ (MW)	Iterations	Termination	Time (s)
26.45	18	Opt	55.13

C. 69-Bus System Results.

The results for the 69-Bus system test case can be seen in Tables V, VI, and VII. From the results, it can be seen that in all scenarios, HT utilisation allows for greater DG implementation while preventing voltage violations. However, the choice of weights impacts the extent of which the HT OPF can utilise HT compensation, which can impact how much additional DG output can be achieved. For example, in the scenarios where $w_1 = 0.01$, HT voltage compensation is minimised to such an extent that it is not utilised at all, which results in less DG output compared to other scenarios. The greatest DG output is achieved in scenario $w_1 = 0$, $w_2 = 0$, where HT compensation is not minimised. In which, the maximum possible amount of DG is achieved, providing an additional 8.05MW of DG to the system, a 30.43% increase compared to the No-HT SLP results. However, it should be noted that in said scenario, since HT compensation is not minimised, HT 3 provides excessive compensation. This is shown in Figure 8, with the voltage magnitude levels for bus 65 being reduced further beyond than what is necessary to prevent voltage violations. In this case, the excessive use of HTs is not major, and as such, does not lead to premature SLP termination. However, this cannot be guaranteed for other networks/test cases, therefore, it is still recommended that HT compensation be minimised to help prevent excessive use of HTs, and premature SLP termination.

In all scenarios, the HT SLP took longer to solve than the No-HT SLP. Furthermore, in most scenarios the HT SLP terminated due to step-size limits being met, as opposed to the No-HT SLP which terminated because a local optimal solution was found. However, even in instances where a local optimal was not found, HT utilisation leads to greater DG output compared to the No-HT SLP results.

These results demonstrate that the HT SLP is capable of successfully utilising HT PIMs to allow for more DG without any voltage violations, provided that appropriate values for w_1 and w_2 are utilised. As such, it has been determined that for the 69-Bus system test case the HT SLP was successful at coordinating multiple HT models.

D. European Low Voltage Test Feeder Results

The results for the Reduced EULV test feeder test case are shown in Tables VIII, IX, and X. From the results, it can be seen that in all cases, HT utilisation allows for greater implementation of DGs while preventing voltage violations. In most cases the maximums possible DG output is achieved,

TABLE VI: 69-Bus System HT SLP Results

w_1	w_2	$\sum_{i\in\mathcal{N}^{DG}}\sum_{\phi\in\Omega} P_{i,\phi}^{DG}$ (MW)	Iterations	Termination	Time (s)
0	0	34.5	14	Opt	80.10
0	0.01	33.15	49	Stp	257.27
0	0.001	34.2	19	Stp	117.53
0.01	0	27.03	19	Stp	85.99
0.01	0.01	27.03	19	Stp	89.01
0.01	0.001	27.03	19	Stp	111.26
0.001	0	34.3	17	Stp	108.91
0.001	0.01	34.13	16	Stp	103.44
0.001	0.001	34.13	16	Stp	102.61

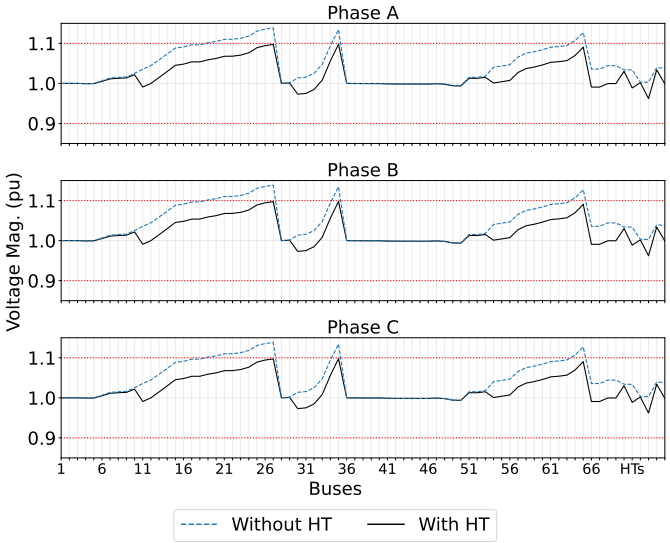

Fig. 8: Voltage magnitude levels of the 69-Bus system with and without HT compensation after 34.5MW of DG has been added (for scenario $w_1 = 0$, $w_2 = 0$).

and an additional 40.39kW can be added into the system, a 28.93% increase from the No-HT SLP results. All HT SLP results were found in fewer iterations than the No-HT SLP results, however, with the exclusion of scenarios $w_1 = 0$, $w_2 = 0.1$, and $w_1 = 0.01$, $w_2 = 0.1$, all HT SLPs took longer to solve than the No-HT SLP. Furthermore, most HT SLPs terminated as a result of the step-size limits being met, as opposed to the No-HT SLP which terminated due to an optimal solution being found. However, despite not reaching an optimal solution, all of the HT SLPs that terminated due to step-size limits still managed to increase DG output, and, with the exception of scenario $w_1 = 0$, $w_2 = 0.01$, allow for the maximum amount of DG.

As shown in Table X, the values chosen for weights impacts how the HT OPF utilises HT compensation to maximise DG. For all cases where $w_1 = 0$, HT compensation exceeds what is required to prevent voltage violations. Such excessive utilisation of HT compensation leads to premature HT SLP termination (as previously described in Section III) in scenario $w_1 = 0$, $w_2 = 0.01$, where $\sum_{i\in\mathcal{N}^{DG}}\sum_{\phi\in\Omega} P_{i,\phi}^{DG}$ is smaller than it is for other HT SLP results, as shown in Table IX. Furthermore, it is also shown that for all scenarios

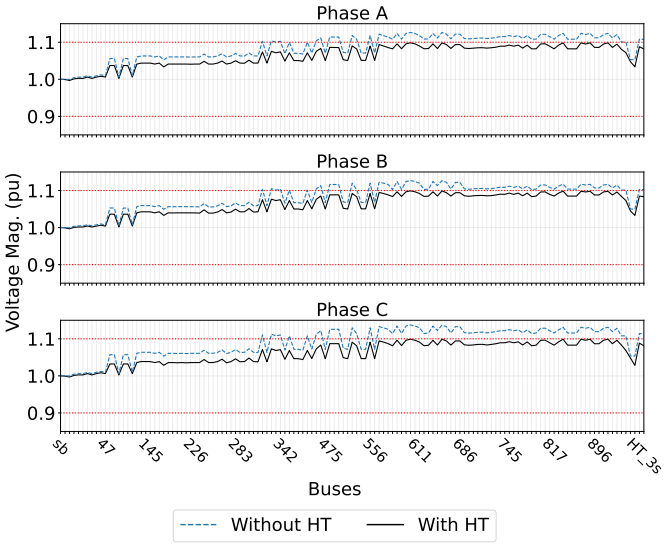

Fig. 9: Voltage magnitude levels of the Reduced EULV test feeder with and without HT compensation after 180kW of DG has been added (for scenario $w_1 = 0.1$, $w_2 = 0.01$).

where $w_1 > 0$, and $w_2 \geq w_1$, voltage compensation provided by HTs 2 and 3, and HT reactive power compensation are not greatly utilised. Instead, greater voltage compensation is provided by HT 1. A more even utilisation of HTs is shown in scenarios where $w_1 > 0$, and $w_2 < w_1$.

In all scenarios, voltage violations are prevented. The best demonstrations are provided by scenarios where $w_1 > 0$, due to HT compensation not being excessively utilised. Figure 9 demonstrates the impact that the HT compensation provided in scenario $w_1 = 0.1$, $w_2 = 0.01$ has on network voltage magnitude levels.

These results demonstrate that the HT SLP is capable of successfully utilising HT PIMs to allow for more DG without any voltage violations, provided that appropriate values for w_1 and w_2 are utilised. As such, it has been determined that for the Reduced EULV test feeder test case the HT SLP was successful at coordinating multiple HT models.

V. CONCLUSION.

This paper proposed an SLP method that can control and coordinate HTs in 3-phase distribution networks without violating network constraints. Test case results demonstrate that the proposed HT SLP method can work in an unbalanced distribution network to successfully reduce the curtailment of DG units, provided that appropriate weight values are applied to the objective function. In addition, test case results demonstrate that the proposed HT SLP method addresses the nonlinearities of the HT PIM formulae while maintaining an acceptable level of accuracy. The proposed HT SLP method has proven that HT coordination is a viable method for allowing for greater DG utilisation in distribution networks.

TABLE VII: 69-Bus System HT Compensation.

Weights		HT 1						HT 2						HT 3					
w_1	w_2	$\lvert v_a^{pq}\rvert$ (pu)	$\lvert v_b^{pq}\rvert$ (pu)	$\lvert v_c^{pq}\rvert$ (pu)	Q_a^{sh} (kVAR)	Q_b^{sh} (kVAR)	Q_c^{sh} (kVAR)	$\lvert v_a^{pq}\rvert$ (pu)	$\lvert v_b^{pq}\rvert$ (pu)	$\lvert v_c^{pq}\rvert$ (pu)	Q_a^{sh} (kVAR)	Q_b^{sh} (kVAR)	Q_c^{sh} (kVAR)	$\lvert v_a^{pq}\rvert$ (pu)	$\lvert v_b^{pq}\rvert$ (pu)	$\lvert v_c^{pq}\rvert$ (pu)	Q_a^{sh} (kVAR)	Q_b^{sh} (kVAR)	Q_c^{sh} (kVAR)
0	0	0.043	0.043	0.043	-287.13	-287.13	-287.13	0.042	0.042	0.042	-468	-468	-468	0.035	0.035	0.036	-338.61	-338.59	-338.48
0	0.01	0.044	0.033	0.037	0	-291.04	0	0.031	0.031	0.044	-21.49	-480.15	0	0.029	0.024	0.031	0	-342.75	0
0	0.001	0.039	0.036	0.035	-156.56	-290.15	-291.17	0.042	0.041	0.042	0	-467.95	-318.98	0.030	0.025	0.025	0	-342.03	-335.61
0.01	0	0	0	0	-297	-297	-297	0	0	0	-495	-495	-495	0	0	0	-346.50	-346.50	-346.50
0.01	0.01	0	0	0	-297	-297	-297	0	0	0	-495	-495	-495	0	0	0	-346.50	-346.50	-346.50
0.01	0.001	0	0	0	-297	-297	-297	0	0	0	-495	-495	-495	0	0	0	-346.50	-346.50	-346.50
0.001	0	0.038	0.039	0.039	-288.15	-287.70	-287.70	0.040	0.042	0.041	-465.37	-464.77	-465.28	0.025	0.026	0.026	-342.07	-341.42	-341.41
0.001	0.01	0.038	0.039	0.039	-289.85	-289.65	-289.65	0.041	0.042	0.041	-472.10	-473.97	-473.24	0.025	0.026	0.026	-341.98	-341.42	-341.42
0.001	0.001	0.038	0.039	0.039	-289.85	-289.65	-289.65	0.041	0.042	0.041	-472.10	-473.97	-473.24	0.025	0.026	0.026	-341.98	-341.42	-341.42

TABLE VIII: Reduced EULV Test Feeder No-HT SLP Results

$\sum_{i\in\mathcal{N}^{DG}}\sum_{\phi\in\Omega} P_{i,\phi}^{DG}$ (kW)	Iterations	Termination	Time (s)
139.61	15	Opt	99.90

TABLE IX: Reduced EULV Test Feeder HT SLP Results

w_1	w_2	$\sum_{i\in\mathcal{N}^{DG}}\sum_{\phi\in\Omega} P_{i,\phi}^{DG}$ (kW)	Iterations	Termination	Time (s)
0	0	180	11	Opt	108.90
0	0.1	180	11	Opt	95.56
0	0.01	153.53	11	Stp	142.16
0.1	0	180	11	Stp	141.65
0.1	0.1	180	11	Stp	138.06
0.1	0.01	180	11	Stp	139.50
0.01	0	180	11	Stp	140.29
0.01	0.1	180	11	Opt	89.18
0.01	0.01	180	11	Stp	137.81

APPENDIX A
NO-HT SLP.

The No-HT SLP is similar to the HT SLP, and is also partially based on the SLP method described in [30] (however, using step-size restrictions as opposed to euclidean distance constraints), making the No-HT SLP method a relatively state-of-the-art distribution optimal power flow method. However, since the No-HT SLP does not utilise HT models, there is no need for the 'HT Accuracy Check' or to adjust HT step-sizes. Furthermore, since there are no HT step-sizes to take into consideration, the No-HT SLP can only terminate if a local optimum solution is found or if the maximum number of iterations is exceeded.

The OPF used for the No-HT SLP is shown below:

$$\max \sum_{i\epsilon N_{DG}} \sum_{\phi\epsilon\Omega} P_{i,\phi}^{DG} \tag{29.1}$$

s.t.

$$\Delta p_{i,\phi}^{Y} = 0, \tag{29.2}$$

$$\Delta q_{i,\phi}^{Y} = 0, \forall i \ \epsilon \ N^{Y} \backslash N^{DG}, \forall \phi \ \epsilon \ \Omega. \tag{29.3}$$

(22.2)-(22.13) and (22.16)-(22.19).

REFERENCES

[1] S. Bala, D. Das, E. Aeloiza, A. Maitra, and S. Rajagopalan, "Hybrid distribution transformer: Concept development and field demonstration," in *ECCE*, Raleigh, NC, USA, Sep. 2012, pp. 4061–4068.

[2] J. Burkard and J. Biela, "Evaluation of topologies and optimal design of a hybrid distribution transformer," in *EPE-ECCE Europe*, Geneva, Switzerland, Sep. 2015.

[3] L. Zheng, A. Marellapudi, V. R. Chowdhury, N. Bilakanti, R. P. Kandula, M. Saeedifard, S. Grijalva, and D. Divan, "Solid-state transformer and hybrid transformer with integrated energy storage in active distribution grids: Technical and economic comparison, dispatch, and control," *IEEE JESTPE*, vol. 10, no. 4, pp. 3771–3787, Aug. 2022.

[4] S. Foti, S. D. Caro, A. Testa, L. D. Tornello, G. Scelba, and M. Cacciato, "An open-end winding hybrid transformer," in *SPEEDAM*, Sorrento, Italy, Jun. 2020, pp. 173–177.

[5] IEA, "Renewables 2023," available at https://www.iea.org/reports/renewables-2023/electricity, accessed 27.03.2024.

[6] J. Burkard and J. Biela, "Hybrid transformers for power quality enhancements in distribution grids - comparison to alternative concepts," in *NEIS 2018 - Conf. Sustainable Energy Supply and Energy Storage Systems*, Hamburg, Germany, Sep. 2020, pp. 112–117.

[7] P. Winter, J. M. Cajigal-Nunez, H. Wrede, and J. Schnepp, "New topology and functionalities of a hybrid transformer for flexible operation of distribution and transmission systems," in *EPE '19 ECCE Europe*, Genova, Italy, Sep. 2019, pp. 1–10.

[8] M. Eremia and M. Shahidehpour, "On-load tap changing transformers," in *Handbook of Electrical Power System Dynamics: Modeling, Stability, and Control*. Wiley, 2013, ch. 7.2.3. On-Load Tap Changing Transformers", pp. 352–371.

[9] J. E. Huber and J. W. Kolar, "Applicability of solid-state transformers in today's and future distribution grids," *IEEE Trans. Smart Grid*, vol. 10, no. 1, pp. 317–326, Jan. 2019.

[10] D. Divan and P. Kandula, "Distributed power electronics: An enabler for the future grid," *CPSS TPEA*, vol. 1, no. 1, pp. 57–65, Dec. 2016.

[11] F. Katiraei and J. R. Agüero, "Solar PV integration challenges," *IEEE Power and Energy Magazine*, vol. 9, no. 3, pp. 62–71, May 2011.

[12] S. Bhattacharya, "Transforming the transformer," *IEEE Spectr.*, vol. 54, no. 7, pp. 38–43, Jul. 2017.

[13] M. Liserre, G. Buticchi, M. Andresen, G. D. Carne, L. F. Costa, and Z. X. Zou, "The smart transformer: Impact on the electric grid and technology challenges," *IEEE Ind. Electron. Mag.*, vol. 10, no. 2, pp. 46–58, Jun. 2016.

[14] M. S. Mollik, M. A. Hannan, M. S. Reza, M. S. A. Rahman, M. S. H. Lipu, P. J. Ker, M. Mansor, and K. M. Muttaqi, "The advancement of solid-state transformer technology and its operation and control with power grids: A review," *Electronics (Switzerland)*, vol. 11, no. 17, Sep. 2022.

[15] T. Guillod, F. Krismer, and J. W. Kolar, "Protection of mv converters in the grid: The case of mv/lv solid-state transformers," *IEEE JESTPE*, vol. 5, no. 1, pp. 393–408, Mar. 2017.

[16] U. Mehrotra, B. Ballard, and D. C. Hopkins, "Bidirectional solid-state circuit breaker using super cascode for mv sst and energy storage systems," *IEEE JESTPE*, vol. 10, no. 4, pp. 3652–3661, Aug. 2022.

[17] A. Carreno, M. Perez, C. Baier, A. Huang, S. Rajendran, and M. Malinowski, "Configurations, power topologies and applications of hybrid distribution transformers," *Energies*, vol. 14, no. 5, pp. 1–35, Feb. 2021.

[18] M. Bazrafshan, N. Gatsis, and H. Zhu, "Optimal power flow with step-voltage regulators in multi-phase distribution networks," *IEEE TPWRS*, vol. 34, no. 6, pp. 4228–4239, Nov. 2019.

[19] M. Bazrafshan, N. Gatsis, and H. Zhu, "Optimal tap selection of step-voltage regulators in multi-phase distribution networks," in *PSCC*, Dublin, Ireland, Jun. 2018.

TABLE X: Reduced EULV HT Compensation.

Weights		HT 1						HT 2						HT 3					
w_1	w_2	$\lvert v_a^{pq}\rvert$ (pu)	$\lvert v_b^{pq}\rvert$ (pu)	$\lvert v_c^{pq}\rvert$ (pu)	Q_a^{sh} (kVAR)	Q_b^{sh} (kVAR)	Q_c^{sh} (kVAR)	$\lvert v_a^{pq}\rvert$ (pu)	$\lvert v_b^{pq}\rvert$ (pu)	$\lvert v_c^{pq}\rvert$ (pu)	Q_a^{sh} (kVAR)	Q_b^{sh} (kVAR)	Q_c^{sh} (kVAR)	$\lvert v_a^{pq}\rvert$ (pu)	$\lvert v_b^{pq}\rvert$ (pu)	$\lvert v_c^{pq}\rvert$ (pu)	Q_a^{sh} (kVAR)	Q_b^{sh} (kVAR)	Q_c^{sh} (kVAR)
0	0	0.066	0.067	0.066	3.42	3.49	-2.78	0.065	0.066	0.066	-3.84	3.72	-3.13	0.066	0.066	0.066	3.89	3.89	-3.6
0	0.1	0.033	0.055	0.055	0	0	0	0.034	0.033	0.008	0	0	0	0.006	0.033	0.033	0	0	0
0	0.01	0.001	0.032	0.035	-3.95	-3.87	3.84	0.054	0.012	0.012	-3.80	-3.95	3.95	0.032	0.011	0.013	-3.93	-3.96	3.96
0.1	0	0.013	0.011	0.020	-3.95	-3.96	-3.92	0.009	0.012	0.015	-3.96	-3.95	-3.94	0.005	0	0.007	-3.96	-3.96	-3.96
0.1	0.1	0.021	0.014	0.023	0	0	0	0.006	0.012	0.013	-2.36	-3.95	-3.95	0.002	0	0.005	-3.96	-3.96	-3.96
0.1	0.01	0.013	0.011	0.020	-3.95	-3.96	-3.92	0.009	0.012	0.015	-3.96	-3.95	-3.95	0.005	0	0.007	-3.96	-3.96	-3.96
0.01	0	0.013	0.011	0.020	-3.95	-3.96	-3.92	0.009	0.012	0.015	-3.96	-3.95	-3.94	0.005	0	0.007	-3.96	-3.96	-3.96
0.01	0.1	0.027	0.025	0.033	0	0	0	0.003	0.006	0.009	0	0	0	0	0	0.002	0	0	0
0.01	0.01	0.021	0.014	0.023	0	0	0	0.006	0.012	0.013	-2.36	-3.95	-3.95	0.002	0	0.005	-3.96	-3.96	-3.96

[20] B. A. Robbins, H. Zhu, and A. D. Dominguez-Garcia, "Optimal tap setting of voltage regulation transformers in unbalanced distribution systems," *IEEE TPWRS*, vol. 31, no. 1, pp. 256–267, Jan. 2016.

[21] J. Zhao, X. Liu, C. Lin, and W. Wei, "Three-phase unbalanced voltage/var optimization for active distribution networks," in *PESGM*, Boston, MA, USA, Jul. 2016.

[22] P. Szczesniak and J. Kaniewski, "Three-phase power flow controller based on hybrid transformer with matrix converter," in *CPE-POWERENG*, Bydgoszcz, Poland, Jun.-Jul. 2016, pp. 250–255.

[23] Y. H. Song and J. Y. Liu, "Steady-state analysis and control," in *Flexible AC Transmission Systems (FACTS)*. IET, 1999, ch. 9, pp. 350–383.

[24] L. Gyugyi, "Unified power flow controller," in *Advanced Solutions in Power Systems: HVDC, FACTS, and Artificial Intelligence: HVDC, FACTS, and Artificial Intelligence*. Wiley, 2016, ch. 10, pp. 559–628.

[25] J. C. Das, "Three-phase models of transformers and conductors," in *Understanding Symmetrical Components for Power System Modeling*. Wiley, 2016, ch. 5, pp. 91–102.

[26] A. Bernstein, C. Wang, E. Dallanese, J. Y. L. Boudec, and C. Zhao, "Load flow in multiphase distribution networks: Existence, uniqueness, non-singularity and linear models," *IEEE TPWRS*, vol. 33, no. 6, pp. 5832–5843, Nov. 2018.

[27] A. Bernstein and E. Dall'anese, "Linear power-flow models in multiphase distribution networks," in *ISGT-Europe*, Turin, Italy, Sep. 2017.

[28] M. Bazrafshan and N. Gatsis, "Convergence of the z-bus method for three-phase distribution load-flow with zip loads," *IEEE TPWRS*, vol. 33, no. 1, pp. 153–165, Jan. 2018.

[29] M. Bazrafshan and N. Gatsis, "Comprehensive modeling of three-phase distribution systems via the bus admittance matrix," *IEEE TPWRS*, vol. 33, no. 2, pp. 2015–2029, Mar. 2018.

[30] A. Bernstein, C. Wang, and J. Y. L. Boudec, "Multiphase optimal and non-singular power flow by successive linear approximations," in *PSCC*, Dublin, Ireland, Jun. 2018.

[31] T. Morstyn, K. A. Collett, A. Vijay, M. Deakin, S. Wheeler, S. M. Bhagavathy, F. Fele, and M. D. McCulloch, "Open: An open-source platform for developing smart local energy system applications," *Appl. Energy*, vol. 275, Oct. 2020.

[32] M. E. Baran and F. F. Wu, "Optimal capacitor placement on radial distribution systems," *IEEE Trans. Power Delivery*, vol. 4, no. 1, pp. 725–734, Jan. 1989.

[33] H. M. Rodrigues Junior, I. D. Melo, and E. G. Nepomuceno, "An interval power flow for unbalanced distribution systems based on the three-phase current injection method," *IJEPES*, vol. 139, Jul. 2022.

[34] K. P. Schneider, B. A. Mather, B. C. Pal, C. W. Ten, G. J. Shirek, H. Zhu, J. C. Fuller, J. L. Pereira, L. F. Ochoa, L. R. D. Araujo, R. C. Dugan, S. Matthias, S. Paudyal, T. E. McDermott, and W. Kersting, "Analytic considerations and design basis for the IEEE distribution test feeders," *IEEE TPWRS*, vol. 33, no. 3, pp. 3181–3188, May 2018.